

Fermionic SK-models with Hubbard interaction: Magnetism and electronic structure

R. Oppermann¹ and D. Sherrington²¹ Institut f. Theoretische Physik, Universität Würzburg, Am Hubland, 97074 Würzburg, FRG² Department of Physics, University of Oxford, Theoretical Physics, 1 Keble Road, Oxford OX1 3NP, UK
(July 26, 2002)

71.10.Fd, 71.23.An, 75.10.-b

Models with range-free frustrated Ising spin interaction and additional Hubbard interaction are treated exactly by means of the discrete time slicing method of Grassmann field theory. Critical and tricritical points, spin- and charge correlations, and the fermion propagator, are derived as a function of temperature, chemical potential μ , of the Hubbard coupling U , and of the spin glass energy J . U is allowed to be either repulsive ($U > 0$) or attractive ($U < 0$). Cuts through the multi-dimensional phase diagram are obtained. Analytical and numerical evaluations take important replica symmetry breaking (RSB)-effects into account. Results for the ordered phase are given at least in one-step approximation (1RSB), for $T = 0$ we report the first two-, three-, and four-step calculations (4RSB) for fermionic spin glasses. The use of exact relations and invariances under RSB together with 2RSB-calculations for all fillings and 4RSB-solutions for half filling allow to model exact solutions by interpolation. For $T = 0$, our numerical results provide strong evidence that the exact spin glass pseudogap obeys $\rho(E) = c_1 E^2 - E_F$ for energies close to the Fermi level with $c_1 \approx 0.13$. Rapid convergence of $\rho(E_F)$ under increasing order of RSB is observed and $\rho(E)$ is evaluated to estimate subleading powers. Over a wide range of the pseudogap and after a small transient regime $\rho(E)$ regains a linear shape with larger slope and a small S-like perturbation. The leading term resembles the Efros-Shklovskii Coulomb pseudogap of two-dimensional localized disordered fermionic systems. Beyond half filling we obtain a $\rho(E) \propto (U)^2$; U ; dependence of the fermion filling factor ν . We find a half filling transition between a phase for $U > U_c$, where the Fermi level lies inside the Hubbard gap, into a phase where $(U < U_c)$ is located at the center of the upper spin glass pseudogap (SG-gap). For $U > U_c$ the Hubbard gap combines with the lower one of two SG-gaps (phase I), while for $U < U_c$ it joins the sole SG-gap which exists in this half-filling regime (phase II). Shoulders of the combined gaps are shaped by RSB due to spin glass order. We predict scaling behaviour at the half filling transition which becomes continuous due to 1RSB. Implications of the half-filling transition between the deeper insulating phase II and phase I for the eventual delocalization by additional hopping processes in itinerant model extensions are discussed. Possible metal-insulator transition scenarios are described. Generalizations to random Hubbard coupling and alloy models as well as frustrated magnetic interactions with ferro- or antiferromagnetic components are also considered separately.

I. INTRODUCTION

The interplay between complex magnetic order and electronic properties including transport attracts growing interest despite an already long history of active and successful research in this field. Reviews of many physical phenomena which result from competing interactions in frustrated magnetic systems can be found for example in Ref. 1 while coupling with electronic transport is discussed in Ref. 2. The particular role of Hubbard interactions in the context of glassy order was considered for random transition metal alloys in Ref. 3 already more than three decades ago. This work described the multiple competition between different interactions, which link magnetism with electronic transport such as mobile carriers in contact with spin glass order, and noted also the interference of the Kondo effect. Moreover an analogy with Anderson localization theory was formulated. At that time the theory of Anderson localization continued to progress over many years and was finally shaped in its replicated field theoretic version in the early eighties, while, independently and almost simultaneously with this event, Parisi discovered the highly complex replica symmetry broken solution of range-free spin glass order^{4,5}. These theories remained remarkably disconnected for a long time, if one disregards for example the analogy discussed in Ref. 3. On one hand, one knew that the unitary universality class of Anderson localization takes into account broken time-reversal invariance in the case of random magnetic scattering centers. However this class, derived for noninteracting disordered systems, cannot simply be assumed to describe localization of charge carriers due to their exposure to spin glass order, which itself is an effect of magnetic interaction. While the potential power of random magnetic order to localize charge carriers is evident, the specific part played by the many body interactions, which can create gaps in the density of states near the Fermi

level and other complicated fluctuation effects, must also be taken care of. A well-known case where disorder and interaction are essential is that of Mott-Anderson transitions⁶. The role of magnetic fluctuations due to singularities in the triplet channel remain a matter of concern. In recent years, the Mott transition of the Hubbard model, ignoring the long-range Coulomb interaction, raised a lot of interest too^{7,8}. The theory of insulators and in particular of antiferromagnetic materials is to a large extent connected with the Hubbard model. The apparent link between magnetism and transport properties and the presence of a metal-insulator transition renders the model particularly attractive. Far from simple however is the many body theory and even the mean field theory of the Hubbard model⁹. Expansions around its local, so-called atomic, limit have been elaborated by Metzner¹⁰. The necessity to generate the effective magnetic interactions and to calculate their magnetic effects in cooperation with transport properties on the basis of the simple atomic limit requires a lot from a perturbation technique. Effective magnetic interaction models were also derived, for example the famous t-J model, which project onto a subset of relevant variables.

An example which combines, on the same footing, the Hubbard interaction with magnetic effects of a (nonlocal) spin interaction, was introduced in Ref. 11 and found necessary in order to deal with weak localization in He³. Our present paper introduces and analyzes a model defined by the grand-canonical Hamiltonian

$$H = U \sum_i n_{i\uparrow} n_{i\downarrow} + \sum_{(ij)} J_{ij} s_i \cdot s_j + \sum_i \epsilon_i n_i \quad (1)$$

where the (ij) run over all pairs and the random magnetic interaction involves Gaussian distributed independent couplings J_{ij} . Spin and charge operators $s_i = n_{i\uparrow} - n_{i\downarrow}$ and $n = c^\dagger c$ are given in terms of fermion operators c . The Hubbard interaction is nonrandom (except in a final section X). The model aims at the description of insulating phases, where the leading role is played by the cooperation of Hubbard- and frustrated spin-interactions. One can view the model as the localized limit of a Hubbard model with frustrated spin interactions and hence, in addition, as a starting point with highly nontrivial magnetic behaviour for expansions with respect to electron hopping. We show that the model is soluble for range-free J_{ij} to the extent that one can derive the full replica symmetry broken solution. The study of such insulating models, or of the insulating side of itinerant models, helps to analyze the precursor of the onset of transport-related phenomena which depend on the interplay between magnetism and energy gaps (in particular at the Fermi level). The breakdown of magnetism and a subsequent and related closing of the gap, when hopping is added, can induce an insulator-metal transition.

Another goal of the research presented in this paper is to study the enhancement of insulating properties and the transition between distinguishable types of insulating phases. The enhancement we find here originates in a constructive superposition of gap widths. It is in general of considerable technological relevance to identify all elementary interaction mechanisms which reinforce or change in a controlled way the insulating tendency of materials and, at the same time, to find relationships with magnetic order. Random magnetic interactions deepen insulating properties by strong density of states depletion near the Fermi level and in addition by the randomness which generates a different type of Anderson localization.

The present work reports progress in understanding insulating fermionic models which incorporate Hubbard interactions in the fermionic extension of the range-free Sherrington-Kirkpatrick spin glass interaction (SK-model)^{2,12,13}. We note in passing that the model contains as special cases not only the standard SK-model (at imaginary chemical potential $\mu = iT=2$) and the atomic limit of the Hubbard model, but also the Ghatik-Sherrington (spin 1) model¹⁴ and of course, for vanishing Hubbard interaction, the fermionic SK-model, which was analyzed in Ref. 15 on 1RSB-level. When a strong Hubbard repulsion effectively evacuates double occupied sites the model operates in an almost three-state per site space. In this regime it is also similar to the model of randomly placed strong U -scattering centers¹⁶ provided the fermions are localized.

The article is organized in three main parts A-C and two additional ones D;E. Part A is purely analytical, while B and C contain the numerical analyses of the exact selfconsistent equations obtained from A. In particular, the reader will find in

A) [section II] the derivation of the analytic solution by means of the discrete time slicing method, where all fields representing the Hubbard interaction are integrated out in perfect coexistence with the spin glass related fields,

B) [sections III-V II]- a detailed numerical analysis of critical and tricritical temperatures, cuts through the multidimensional phase diagram, solutions of the coupled selfconsistent integral equations in the ordered phase, their subsequent use in the calculation of the fermion propagator including the density of states and a calculation of the fermion concentration, all given as a function of the chemical potential. The full range of μ for which the spin glass phase can exist is covered. Particular attention is paid to the large replica symmetry breaking (RSB-) effects at low temperatures including $T = 0$. For $T = 0$ we present the first 2-step RSB-evaluation for fermionic spin glasses (with arbitrary filling),

C) [section V III] the 4-step RSB solutions for half filling which lead, by interpolation with known exact relations, to a prediction of the exact form of the spin glass pseudogap. The nonanalytic behaviour is determined and a comparison

with the Efros-Shklovskii Coulomb pseudogap included.

In the remaining smaller part D randomness in the Hubbard coupling is included in order to control changes in the domain of discontinuous and continuous phase transitions, and finally in E, implications of the gap structure derived in part B are discussed. In particular we include in

D) [section IX] a phenomenological discussion of the onset of diffusive transport beyond a metal-insulator transition. Two scenarios for metal-insulator transitions governed by the random and frustrated magnetic interaction of spin glasses are described. This part serves to describe one of the major aims of our current research. Finally in

E) [section X, XI] the effect of several distributions of random Hubbard interaction on the freezing temperature T_f are analyzed, and a discussion of ferro- or antiferromagnetic effects induced by nonzero mean values of J_{ij} concludes the paper.

Continued efforts to approach the (best possible) analytical $T = 0$ -solution for the mean field theory of non-itinerant spin glasses form a part of the paper. Sufficiently good qualitative, if not quantitative, knowledge of this localized $T = 0$ solution seems necessary, or at least a helpful basis for the analysis of itinerant glassy magnetism in fermionic systems. This can easily be understood if one reviews the strong low temperature RSB-effects on relevant properties (like shape, effective width, and stability against thermalizing) of gaps in the band structure. Pseudogaps at the Fermi level or smallness of the density of states in the vicinity of E_F are features which undoubtedly are relevant for two-particle correlation functions such as conductivities. For this reason RSB has the power to influence $T = 0$ phase transitions and must be controlled, in particular with respect to predictions for metal-insulator transitions. It is also interesting to compare our results with spin dynamical fluctuation effects in disordered or translationally invariant quantum spin systems. Unfortunately (in the sense of solvability) $T = 0$ phase transitions often occur as quantum spin glass transitions which involve utterly complicated connections between quantum spin dynamics, critical behaviour and RSB.

Implications of RSB in many body quantum physics have not yet been sufficiently explored. We mention two examples: i) localization theory involves non self-averaging quantities and a RSB-free theory is questionable with respect to these observables, and ii) recent theories of quantum critical points in low-dimensional transverse field Ising systems have shown the importance of infinite-disorder fixed points¹⁷, which were expected to be applicable to quantum spin glass transitions as well. Their relevance in high dimensions (domain of attraction) and even in mean-field limits must be analyzed. Although the comparison between non-replicated and replicated methods is often difficult, the claim of relevance of strong coupling theories can well be related to the strong coupling theory needed to incorporate complete RSB, which was a motivation of the present research. We cannot answer these questions in the present paper, but our attempt to find analytical solutions at $T = 0$ for the present infinite-range problem is also meant as a step towards infinite-dimensional systems and the control of RSB-relevance. If one wants to understand the term 'relevance' in the renormalization-group sense, it is important that continuous $T = 0$ phase transitions can exist in the system. While the magnetic breakdown is discontinuous in the mean field case and probably in general too, we derive and emphasize the special nature of half-filling transitions of the present model. Moreover this transition is sharp only at $T = 0$ and becomes continuous only due to infinite RSB, while in other cases RSB renders a first order transition even more discontinuous (one example given in Ref. 18).

Also recently and during progress of the present work, a numerical approach using infinite RSB equations¹⁹ was proposed which employs an interesting analogy between the 3SAT-optimization problem^{19;20} and the standard SK-model at $T = 0$. In our approach, apart from considering more general model, we follow a different approach which attempts to evaluate the maximum feasible number of integrations involved in 1 RSB equations. In this paper the highest accuracy is so far the 2RSB-approximation of the exact solution for arbitrary values of the chemical potential and 4RSB for particle hole symmetry $= U=2$ (half filling).

Since the techniques applied in section II are readily extended to include statistical distributions of the Hubbard interaction and/or different interaction strength for A and B-type atoms in A-B alloys we extended our analysis to study models described by the Hamiltonian $H + H$ with

$$H = \sum_i \sum_{\alpha} U_i n_{i\alpha} n_{i\beta}; \quad (2)$$

where U obeys a wide variety of different distributions. We evaluate changes in critical temperatures and their effect on the phase diagram. This part helps to gain insight into the competition between repulsive and attractive interactions on one side and spin glass order on the other. The strong asymmetry between positive and negative U are incorporated in one model and weighted by U -distributions. A distribution-invariant point is found (for symmetric distributions), i.e. a point where the critical temperature does not depend on U -fluctuations at all.

Due to the absence of spin- and charge-quantum dynamics (in the hopping free model) one may expect the model to be more easily solvable than the Hubbard model, the solution of which faces the high obstacle of complicated dynamics. However randomness of the magnetic interaction introduces the complication of replica symmetry breaking

at all temperatures below freezing and in particular at $T = 0$ too. The additional introduction of hopping leads to further complications, since all problems of the Hubbard model are then contained too. Let us mention the two most important classes of itinerant model extensions. These are given by the single-fermion and (fermion)-pair hopping Hamiltonians by

$$\text{a) } H_t = \sum_{(ij)} t_{ij} c_i^\dagger c_j ; \quad \text{b) } H_t^{\text{pair}} = \sum_{(ij)} t_{ij}^{(p)} c_{i\#}^\dagger c_{j\#}^\dagger c_j c_i ; \quad (3)$$

which respectively have the tendency to delocalize single fermions or pairs of fermions. Each of these additional hopping Hamiltonians can be combined with models (1) and (2). In section IX we describe qualitatively effects of the single-fermion hopping term H_t . A perturbation theory in the fermion hopping elements requires detailed (if not exact) knowledge of the fermion propagator in the insulating limit, which is analyzed in section V III C.

The pair-hopping Hamiltonian H_t^{pair} , on the other hand, can cause a coherent pair state with various consequences. Related questions concern the possible existence of microscopic superconducting glasses. An interesting simplification of 3b) if compared to 3a) is the fact that H_t^{pair} commutes with Hamiltonian (1), which means that the spin glass field Q has a static saddle point. Quantum dynamics of the $SU(2)$ generators $c_\#^\dagger c_\#$, $c_\#^\dagger c_\#^\dagger$ does not invalidate a Q -static theory (unlike the H_t Hamiltonian). Since the pair operators are $SU(2)$ generators as well, a distribution of the pair-hopping elements analogous to the J_{ij} in an SK-model would generate an XY superconducting glass model. Its description requires a quantum-dynamic order parameter and thus falls into another class of low temperature behaviour.

Experiments on two-dimensional electron gases (2DEG) with strong ferromagnetic coupling to local moments^{21,22} demonstrated the relation between transport and magnetism in the presence of disorder and correlation. A spectacular giant magnetoresistance was observed in small fields while a transition into a quantum Hall liquid took place at high fields. The 2D-geometries were intentionally used to rule out orbital effects and in Ref. 21 to suppress magnetic order. Results of our paper show that a strong ferromagnetic coupling to a spin glass ordered II-VI semiconductor, for example, would present a novel case with certain new fundamental questions reaching beyond the mere comparison of the difference between paramagnetic- and spin glass response. This experimental situation would test localization mechanisms of more than one kind (and different from the unconfirmed²¹ possibility of polaron formation): given that the strong coupling between 2DEG and randomly oriented magnetic moments support Anderson localization while a spin glass pseudo-gap, which we discuss in this paper in comparison with the Efros-Shklovskii gap, is expected to contribute a particular stretched-exponential low temperature resistance. Moreover the spin glass order does not smear the correlation-induced level correlation, but increases it further as described below.

One final remark refers to the energy scale used in our article: since we focus on the spin glass phase generated by a Gaussian-distributed random spin interaction the most important energy scale is set by $J = \sqrt{\frac{1}{N} \sum_{ij} (J_{ij} - \overline{J_{ij}})^2}$. We work hence in J -normalized dimensionless energy variables in order to ease reading. Only when needed, this normalization is mentioned explicitly.

II. EXACT DERIVATION OF SELFCONSISTENT SCHEMES FOR FRUSTRATED RANGE-FREE MAGNETIC INTERACTION AND HUBBARD INTERACTION

Working the double-interaction model (1) into a replicated Grassmann field theory is a standard procedure. The Grassmann field technique is explained for example in Ref. 23. Usually a continuous time limit is taken before the fermionic fields are integrated out. This involves an unknown infinite constant which is removed by a regularization. The discrete time (slicing method can instead be used and all integrations performed before the continuum time limit is taken at the end. This is known to be the exact procedure of field theory. It avoids singularities of the symbolic continuous time formalism and hence does not require regularization. Its feasibility depends on whether a quadratic form in the Grassmann fields can be obtained and in particular be diagonalized. In spite of an $O(N^8)$ effective spin glass interaction (before decoupling) and the subsequent complication by RSB, we found it convenient to solve the problem in this exact way (up to the analysis of RSB which is the only source of approximations in the paper).

The Hubbard interaction, local in real space and in time, competes with the infinite range SK Hamiltonian and its statistical spin correlations, which are local in time but also involve time-independent (infinite-ranged in time) magnetic disorder correlations. Both interactions can be decoupled altogether. Not only the Grassmann integrals can be performed but also the Hubbard-decoupling fields will be integrated out exactly. This procedure is applied first to the partition function in IIA and subsequently to the fermion propagator in IIB, where it requires a modification. This amounts to a diagonalization of the problem, exempting only the final solution of infinite-step replica symmetry breaking. Reaching a four-step accuracy at $T = 0$ in section V III turns out to be sufficient for drawing the physically relevant conclusions.

The grand canonical partition function of model (1) for fermions in a particle bath with chemical potential can be expressed in terms of the anticommuting eigenvalues a_i^a , a_i^b of the fermion operators c_i, c_i^\dagger . This is achieved by inserting the representation of 1 in terms of fermionic coherent states at $M-1$ equidistant time slices of the imaginary time interval $0 \leq \tau \leq \beta$. The index a denotes an n -fold replication of the system. Then, as usual in the framework of the replica trick, the averaged free energy $F = -\frac{1}{\beta} \ln Z$ is calculated from the disorder average of

$$Z^n = \lim_{M \rightarrow \infty} \frac{1}{M} \int \prod_{i,a} d a_i^a(k) d a_i^b(k) \exp \left[\sum_{a,k=0}^{M-1} K^a(a_i^a(k+1); a_i^a(k)) + K^a(a_i^b(0); a_i^b(M-1)) \right] \exp \left[\sum_{i,a,k=0}^{M-1} \left(a_i^a(k+1) a_i^a(k) - a_i^b(k) a_i^b(0) - a_i^b(M-1) a_i^b(0) \right) \right] \quad (4)$$

where

$$K^a(a_i^a(k+1); a_i^a(k)) = \sum_{(ij)} J_{ij} a_i^a(k+1) a_j^a(k) + \sum_i \frac{U_i}{4} (a_i^a(k+1) a_i^a(k))^2 + \sum_i \frac{U_i}{4} (a_i^b(k+1) a_i^b(k))^2 + \sum_i a_i^a(k+1) a_i^b(k) \quad (5)$$

The disorder average, performed over the chosen Gaussian distribution of frustrated magnetic couplings J_{ij} (but fixed Hubbard-coupling U of arbitrary sign) leads to an effective functional with 8-fermion correlation. This integration and the subsequent decoupling of the 8-fermion interaction (which is equivalent to the usual 4-spin interaction) are standard and not repeated here in detail. We just mention that the Gaussian decoupling by means of fields $Q_i^{ab}(k; k^0)$ initially depend on two times as well as replica labels, since those carry along all degrees of freedom as obvious from the coupling term $Q_i^{ab}(k; k^0) a_i^a(k) a_i^b(k^0)$. The decoupling fields for the Hubbard interaction, expressed above in terms of charge and spin operators, are dynamic; we denote them by q_k and z_k for each time instant k . The spin glass Q -fields can in general also show quantum dynamical behaviour. This would be the case if transport processes were allowed. As in quantum Heisenberg spin glasses²⁴ or e.g. in the famous Hubbard model in infinite dimensions⁷, quantum dynamics poses even a major obstacle in finding an exact analytical mean-field solution. We remark that the present techniques in principle allow to include quantum spin- or charge-dynamical effects but exact solutions may not be found even in the mean-field limit. Here we consider only cases in which the mean of J_{ij} is zero or positive so that in the following decomposition

$$Q_i^{ab}(k; k^0) = q_i^{aa}(k, k^0) + q_i^{ab}(1) + Q_i^{ab}(k; k^0) \quad (6)$$

a saddle point matrix without spatial variation applies, and the site i index has been dropped in its elements q . The spatial dependence of the saddle point solutions must instead be retained in cases like glassy antiferro- or ferrimagnets, two-component magnets¹⁸ or similar phases, where regular spatial structures are not removed by averaging over disorder. In the absence of quantum spin dynamics, as is the case for the present non-itinerant model, the spin glass order parameter fields $Q_{kk^0} = Q_i^{ab}(k; k^0)$ have a purely static saddle point. Thus one can take advantage of the time independence of $q^{aa}(k, k^0) = q$, noting in addition that $q^{ab} = \lim_{t \rightarrow \infty} \langle a_i^a(t) a_i^b(0) \rangle$ is always static unless non-equilibrium dynamics is taken into account. Moreover contributions from Q vanish in the thermodynamic limit. It is worth noting that also in the finite-range extension of the present model a non-dynamic q^{aa} is obtained. In contrast to Heisenberg spin glasses or metallic spin glasses, where the so-called static approximation of $Q^{aa}(t; t^0)$ is in principle inadequate and perhaps fails to detect important features, the present model poses a static average of the diagonal Q -fields – we emphasize that, within the present paper, approximations are only applied in the context of a finite number of replica symmetry breaking steps. At present we implicitly keep complete RSB by means of the Parisi matrix Q_{Parisi} and continue to perform exact operations on the replicated partition function, which is obtained after averaging (4) over a Gaussian distribution of the random magnetic interaction J_{ij} as

$$\langle Z^n \rangle = \text{const} e^{-\frac{1}{4} N \text{Tr} Q_{\text{Parisi}}^2} \int \prod_{a,k} d a_k^a d a_k^b d z_k^{(b_r)} d y_{a,k}^a d y_{a,k}^b d y_{a,k}^c \quad (7)$$

The superscript G stands for normalized Gaussian integrals and $\text{fr};b_r g$ runs over all spin decoupling elds $z_r^{(b_r)}$ on which the effective eld H_{eff} depends. The spin- elds $z_r^{(b_r)}$ serve to decouple all $O(4)$ -terms of the form $(\text{tr})Q_{\text{Parisi}}(\text{tr})$, which are associated with the r -th level block matrices aligned along the diagonal of the Parisi Q -matrix^{4,5}. The crucial tree structure of Parisi-RSB is thus kept track of in the exponent

$$(B) \prod_{r=0}^{b_r+1} \prod_{m_r+1=m_r}^{b_r+1} \prod_{k=0}^{b_r+1} B^{aa} (H_{\text{eff}}(y^a; f z_r^{(b_r)} g))^{a_{k0}} ; a = b_0 \quad (8)$$

where \prod symbolizes a multiple sum over all $b_0; b_1; b_2; \dots; b_1$ with boundary conditions $m_0 = 1$ and $m_1 = n$. Integration over Grassmann elds will readily yield the determinant of B . This matrix is given by

$$(B^{aa})_{k+1;k} = (1 + \frac{p}{i} \frac{1}{U=2} \frac{a}{k} + \frac{h_p}{i} \frac{1}{U=2} \frac{a}{k} + H_{\text{eff}}(y^a; f z_r g)) \quad (9)$$

$$(B^{aa})_{k;k} = 1 \quad \text{and boundary terms } B_{0,M-1} = B_{M,M-1} ; \quad (10)$$

where

$$H_{\text{eff}}(y^a; f z_r g) = \frac{p}{q_1} \frac{1}{q_1} y^a + \sum_{r=1}^X \frac{p}{q_r} \frac{1}{q_{r+1}} z_r^{(b_r)} \quad (11)$$

represents the spin-glass effective eld. The effective eld acquires an additional magnetization contribution $J_0 < \dots >$ in case one allows a finite mean value of $J_0 < J_{ij} >$. Truncating the sum over r after the $q+1$ -th term with $q+1 = 0$ represents the q -step approximation to full RSB, which we call q -RSB and 1-RSB respectively. The Gaussian integral operator representation

$$Z_G = \int \frac{dz}{2\pi} e^{-\frac{z^2}{2}} \quad (12)$$

provides more transparency especially in reading multiple integrals. We use this definition everywhere in the paper. For each replica index a , the Grassmann integration leads to the determinant

$$\det B^{aa} = 1 + \sum_{k=0}^{M-1} \frac{p}{U=2} (i \frac{a}{k} + \frac{a}{k}) + H_{\text{eff}}(y^a; f z_r g) \quad (13)$$

which still depends on the z -(spin)-eld con guration. Time slicing of the imaginary time interval $0 < \dots < \beta$ was performed in $M-1$ equidistant steps of size $\beta = \beta/M$. The continuum time limit and hence the exact solution will result by taking the limit $M \rightarrow \infty$ in the end. Let us further abbreviate by use of the shorthand notation

$$\begin{aligned} Z_G \det B &= \prod_{a,k} \prod_{k'} \prod_{k''} \det B \\ &= (1 + \frac{p}{U=2} (i \frac{a}{k} + \frac{a}{k}) + H_{\text{eff}}) + \frac{p}{U=2} (i \frac{a}{k} + \frac{a}{k}) + H_{\text{eff}} + \frac{p}{U=2} (i \frac{a}{k} + \frac{a}{k}) \\ &+ \frac{p}{U=2} (i \frac{a}{k} + \frac{a}{k})^2 + H_{\text{eff}} + \frac{p}{U=2} (i \frac{a}{k} + \frac{a}{k})^2 \end{aligned} \quad (14)$$

and extract the contributions which survive in the continuum time limit, expressed by $\beta \rightarrow 0; M \rightarrow \infty; \beta/M = \beta$. The integration over the Hubbard decoupling elds can be executed exactly which yields in the continuum time limit

$$\det B = 2e^{-\cosh(\frac{U}{2})} e^{-U/2} + \cosh(H_{\text{eff}}(y^a; f z_r^{(b_r)} g)) \quad (15)$$

Using this result together with Eq.11 and Eq.7 in the expression for the free energy per site (respectively the thermodynamic potential) $F = -T \lim_{n \rightarrow 0} (\ln Z^{(n)})/n$ one finds (after one more integration over the y^a - elds)

$$F = \frac{1}{4} \ln 2 + \frac{1}{2} (q_1 - 1) + \frac{1}{4} \sum_{r=1}^X m_r (q_r^2 - q_{r+1}^2) \ln 2 \quad (16)$$

$$\begin{aligned} & \lim_{r \rightarrow 1} \frac{1}{m_r} \ln \left(\prod_{z_{r+1}} \prod_{z_r} \prod_{z_2} \prod_{z_1} C(f z_r g)^{m_1} g^{m_2=m_1} g^{m_3=m_2} \dots g^{m_r=m_{r-1}} \right) \\ & C(f z_r g) = \cosh(H_{\text{eff}}(0; f z_r g)) + e^{-(U+1)/2} \cosh(\frac{U}{2}) \end{aligned} \quad (17)$$

B. Generating functional for quantum dynamical fermion correlations

The imaginary time single-fermion propagator (and N-fermion propagators too)

$$G_{ij}^{(a)}(k; k^0) = h_i^a(k) j_j^a(k^0) i = i j h_i^a(k) j_j^a(k^0) i \quad (18)$$

can be derived by derivatives with respect to the generating fields from the generating functional

$$(\mathbf{g}_i) = \ln \frac{Y^Z}{D} e^{-B} + \quad (19)$$

Let us symbolize Gaussian integrals over arbitrary decoupling-elds by $\int_{\mathbb{R}^Q}^{\mathbb{R}_G}$, where \mathbb{R}_G stands either for \mathbb{R}^Q -spin or \mathbb{R}^Q -Hubbard-elds, and by $\int_{\mathbb{D}}^{\mathbb{D}}$ for the Grassmann-eld integration. Using

$$\mathbb{Z}^{\mathbb{D} \times \mathbb{E} \times \mathbb{B}^+} = \det \mathbb{B} e^{\mathbb{B}^{-1}} \quad (20)$$

we calculated the inverse matrix B^{-1} in order to obtain the propagator. We choose $\omega > 0$ with $k_z = 0$ and $k_\perp = k_F$ and obtain the (disorder-averaged, local) fermion propagator as

$$G^{(a)}(0) = \lim_{M \rightarrow 0} \left(\frac{Y_{ZG} Y_{ZG} Z_{ZG} Z_{ZG} \#_{Y^1}}{r_{fzrg} a^0 y^a a^0 a^0 k=k_i} + H_{eff}(y^a; fzg) + \frac{r}{2} \frac{U}{U} (i_k^a + i_k^a) \right) \#$$

$$1 + \frac{M_{Y^1}}{k=0} (1 + H_{eff}(y^a; fzg) + \frac{U}{2} (i_k^a + i_k^a)) = N; \quad (21)$$

where $N = \sum_z \sum_y h_Q R_Q R_R R_i$ detB. Splitting the product of the second bracket into one over the interval $k_i; k_f$ and one for the rest, the resulting form allows to solve the Gaussian Hubbard-integrals. Terms of order $3=2$ do not survive the continuum \lim it and the exact solution becomes

$$G^{(a)}(\quad) = \begin{pmatrix} Y & Z & G & Y & Z & G \\ r & f_{Z_r} & g & a^0 & y^{a^0} & \end{pmatrix} (e^{(+H_{eff})} + e^{(-H_{eff})} e^{(+H_{eff}U)}) = N \quad (22)$$

After Fourier transformation from imaginary times to imaginary frequencies ($\omega_n = (2n + 1)T$) the fermion Green function in 1RSB, which illustrates RSB effects on the propagator in a relatively simple form, is obtained as

$$G^{1\text{RSB}}(n) = \int_{z_2}^{z_G} \int_{z^0}^{z_G} C(z^0; z_2)^m \int_{z_1}^{z_G} C(z_1; z_2)^m \int_y^{z_G} \frac{e^{-(U + H_{\text{eff}})} + 1}{i_n + U + H_{\text{eff}}} + \frac{e^{-(H_{\text{eff}})}(e^{-(U + H_{\text{eff}})} + 1)}{i_n + H_{\text{eff}}} dy dz_1 dz_2 dz^0 \quad (23)$$

with normalizing factor $C(z_1; z_2) = 2e^{-(z_1+z_2)/2} C(z_1; z_2)$ and C given by Eq.17. The result reduces to the known limit in case of vanishing effective field $H_{\text{eff}} = 0$ the propagator of the Hubbard model's atomic limit is retrieved⁷ and, for $U = 0$, the fermionic Ising spin glass limit is retained¹⁵. The result Eq.23 displays the U -correlation induced two-level splitting, which is broadened into bands by the statistically distributed spin glass fields $H_{\text{eff}}(z)$. This smearing

of delta-peaks into bands might lead to less singular expansions in powers of hopping terms than those expansions encountered in the pure Hubbard model. We shall further solve below the y -integration for all T and at $T = 0$ also the z_1 -integration in order to get a most explicit analytic form. The remaining numerical task is still not quite easy, since all parameters on which the effective field depends and the Parisi block parameter $m = m(\mu; U; T)$ must first be found as selfconsistent solutions and then used in the calculation of the density of states. As Eq.23 suggests the procedure can be extended to formulate N -particle propagators.

III. DEPENDENCE OF FREEZING TEMPERATURE ON REPULSIVE AND ON ATTRACTIVE HUBBARD COUPLINGS U

The temperature T_f at which spin glass freezing occurs depends on the chemical potential and on the Hubbard coupling U . The reduction of doubly occupied sites under increasing $U > 0$ favors magnetic order and thus counteracts the effect of a growing deviation from particle hole symmetry, described by the parameter $\mu_{PHS} = \frac{1}{2}U$. Thus the freezing temperature tends towards the SK-value in the infinite repulsion limit for fixed μ_{PHS} . On the other hand, negative (attractive) Hubbard interactions act in the same direction as 'particle pressure' from the particle reservoir: both enhance double occupation. At a critical negative U the magnetic phase will break down.

The derivation of the nonperturbative selfconsistent T_f -equation follows the standard procedure for the fermionic generalization of the SK-model. The results of this section identify the regimes of continuous and of discontinuous transitions below a tricritical temperature called T_{f3} .

The selfconsistent equation for the freezing temperature of the infinite range model reads (in units of J)

$$T_f = 1 - (1 + e^{-(1+U)})^{(2T_f)} \cosh((U-2)T_f); \quad (24)$$

which reduces in the special case $U = 0$ and $\mu = 0$ to the standard SK-model result.

The numerical evaluation of T_f for several fixed values of U , including attractive interactions, is displayed in Figure 1. The Figure illustrates the competition between chemical potential and Hubbard repulsion.

The vertical dashed lines at $\mu = U$ drawn in Fig.1 will be found later to represent the exact limit of half-filling at $T = 0$, while particle hole symmetry (not shown in the Figure) lies at $\mu = \frac{1}{2}U$. Figure 1 shows specific cuts through the model's multidimensional phase diagram which provide here a complete picture of its dependence on chemical potential and Hubbard interaction. Only the first order thermodynamic transition lines $T_{f1}(\mu)$ (defined by the crossing of magnetic and nonmagnetic free energies) all resemble the one shown around 10:9 and depend on RSB . They are not yet better determined than in $1RSB$. The back-swing observed for $T_{f1} \rightarrow 0$ may well occur at the crossover temperature where the next higher RSB -step is required. The full RSB -solution is not yet known, but is expected to lie closer to the stability limit. Thus Figure 1 determines the phase diagram's μ -dependence apart from small RSB -corrections near $T_{f1} = 0$. In the large U -limit, the T_f -curve approaches the shape of a box with height 1 and a width given by the value of the chemical potential at the tricritical point. This is obtained in Eq.25 below.

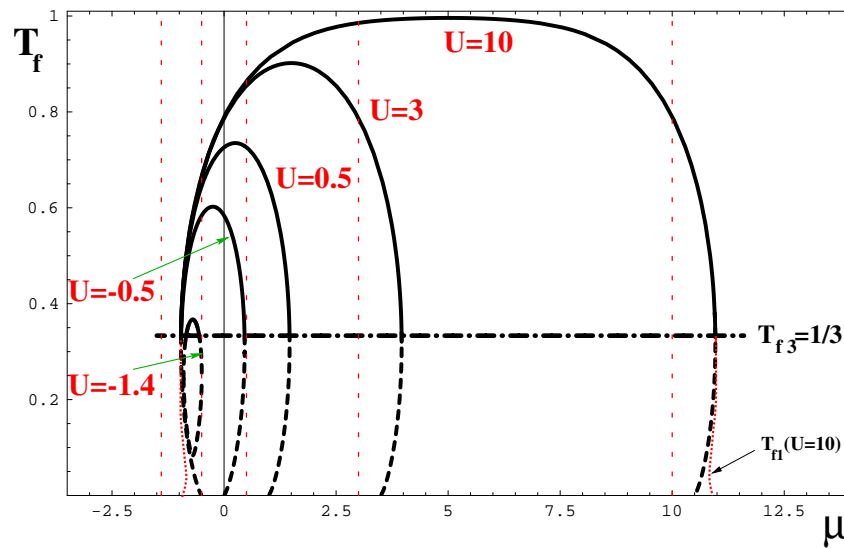


FIG. 1. Phase boundaries of the solutions which extremize the free energy (24), shown as a function of chemical potential μ and for a set of fixed Hubbard couplings $U = -1.4; -0.5; 0.5; 3$, and 10 (in units of J). Solid bold lines are solutions of Eq.(24) in the regime of continuous transitions. Dashed bold lines, beneath the dash-dotted bold tricritical line at $T_{f3} = 1=3$, are solutions of Eq.(24) too but describe paramagnetic only stability limits preempted by first order transitions. First order transition lines, which depend on RSB , are shown for $1RSB$ for $U = 10$. Dashed vertical lines at $\mu = U$ show (as a guide for the eye) how far μ can exceed the Hubbard coupling U (which is also the half-filling limit at $T = 0$) before spin glass order breaks down. Each curve is symmetric with respect to its particle-hole symmetric point at $\mu = U=2$.

A. The tricritical temperature T_{f3} and corresponding chemical potential $\mu_{f3}(U)$

The tricritical temperature, included in Figure 1, appears as the lower limit of second order freezing transitions and remains $\frac{1}{3}$ independent of U . This is readily found by solving Eq 24 together with the condition $\cosh((\mu - U)/2) = T_{f3} = 2 \exp((1+U)/(2T_{f3}))$, where the $O(q^2)$ -term of the order parameter equation changes sign. For deviations from particle hole symmetry (half-filling) which are larger than a tricritical value $j_{f3} = U=2$ given in Eq.(25), the order parameter can no more vanish continuously.

A special feature is the breakdown of spin glass order due to sufficiently strong attractive (negative) U couplings. As Figure 1 shows, minimum values in the range of negative Hubbard couplings U_{min} and of the chemical potential exist, below which a spin glass cannot exist. The tricritical chemical potentials are symmetric with respect to PHS at $\mu = \frac{U}{2}$ and one finds (recalling that T, U are given in units of J)

$$T_{f3}; \mu_{f3}(U) = \frac{U}{2}g = \frac{1}{3}; \quad \frac{1}{3}\text{arccosh}(2e^{3(1+U)/2})g \quad (25)$$

For homogeneous attractive Hubbard interaction

$$U > U_0 = -1 - \frac{2}{3}\ln 2 \quad (26)$$

limits the regime of continuous transitions. In a very small range $U < U_0$ discontinuous transitions still exist.

B. Implications of magnetic breakdown for large negative $U < U_{min}$

The destruction of magnetic order by sufficiently attractive Hubbard interaction is due to a redistribution of density of states. A critically high density of paired states breaks down the magnetic order and in principle would create a coherent superconducting state in cases when fermion hopping- or pair-hopping mechanisms like those given in Eq.3 are present. The nonlocal magnetic interaction J_{ij} by itself can however not generate a coherent superconducting state.

As discussed in a chapter X, J-U models with additional random U and in particular with ($U_A > 0; U_B < 0$) include extreme proximity- (vicinity-) effects between local pairs and local moments on neighboring sites. It will be very interesting to study the instability of such phases towards delocalization by Hamiltonians of the type 3a) and b).

IV. BAND-AND GAP-STRUCTURES IN THE PRESENCE OF FRUSTRATED MAGNETIC ORDER

1. The fermionic density of states of the SK model with Hubbard interaction in replica symmetric approximation

In models as hard to solve as Hubbard- and spin glass models the density of states has the virtue of being one of the simpler quantities with yet a broad physical significance. It is important for many one particle properties. Thermodynamic behaviour as observed in quantities like particle number (as a function of chemical potential), internal energy, specific heat, thermopower etc. depend on it. Detailed properties of the DOS near the Fermi level influence the stability of the insulating phase against fermion hopping processes in itinerant model extensions. Due to the Ward identity for charge conservation³² one finds that the DOS also determines the amplitude of the dispersive two-particle propagator. The DOS can predict the existence of a metal-insulator transition by means of the closing of an energy gap at the Fermi level; however it is insufficient to decide where and under which conditions exactly such a transition takes place, since this requires to calculate the decay of the dispersion constant by means of a two-particle correlation function. It is one goal of the present paper to construct the basis for such calculations.

The replica symmetric approximation is known to be unstable everywhere in the ordered phase (in fermionic extensions

$$\begin{aligned}
\mathcal{H}_0(E) &= \frac{1}{2q} e^{(E+)^2 = (2q)} (\ln [\dots; U \dots = 2] E) \\
&+ e^{(E-U)^2 = (2q)} (E (2U \dots + = 2)) (\dots = 2 E) + e^{(E-U)^2 = (2q)} (E \max[U + \dots; + = 2]);
\end{aligned}
\tag{27}$$

$$q = 1 - j - 1j \quad 1 = \operatorname{erf}\left(\frac{U}{\sqrt{2q}}\right) \quad \left(\frac{U}{\sqrt{2}}\right); \quad = \frac{r}{2} e^{-(U/\sqrt{2})^2 = (2q)} \quad (=2 - U) \quad (28)$$

If $U < \frac{1}{2}$:! three bands for $E < U + \frac{1}{2}$; $2U + \frac{1}{2} < E < \frac{3}{2}$; $E > \frac{3}{2} + \frac{1}{2}$
 If $U > \frac{1}{2}$:! two bands for $E < \frac{1}{2}$; $E > U + \frac{1}{2}$

The full Green function (in the finite temperature technique) is given by the spectral representation $G(\omega) = \frac{1}{\omega - \epsilon_0} + \frac{1}{\omega - \epsilon_1} + \dots$ where $\epsilon_l = (2l+1)T$ and the finite temperature symmetric DOS $\rho_0(E; T)$ is given by

w ith

$$(\cdot; U; T; z) = e^{(U + \cdot) = (2T)} \cosh\left(\frac{U=2}{T}\right) + \cosh\left(\frac{p_{\bar{q}} z}{T}\right) \quad (30)$$

The fermion concentration for given chemical potential is calculated using Eq.(30) in

$$(\rho; U; T) = \int_{-1}^1 dE \frac{1}{e^{(E - \mu)/T} + 1} \quad (E) \quad (31)$$

10

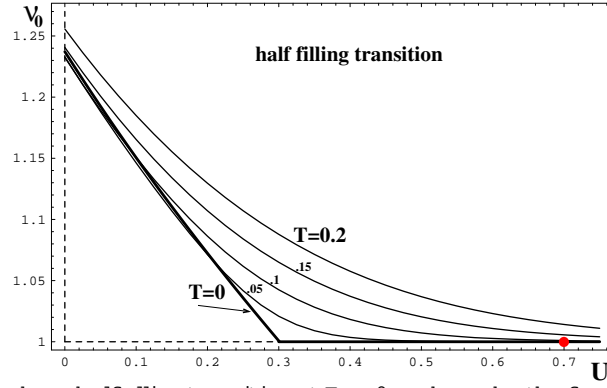


FIG. 2. Thermal smearing of the sharp half filling transition at $T = 0$ as shown by the fermion concentration $\rho_0(T)$ for $\beta = 0.7$ in replica symmetric approximation. Temperatures are given in units of J . The critical Hubbard coupling $U_c = 2$ in ORSB-approximation and its exact position (dot) at $\beta = U$ for vanishing nonequilibrium susceptibility (see below).

One aspect of RSB and of the unbroken approximation becomes obvious from Fig. 2: temperatures above $0.15[J]$ are enough to render RSB-effects small enough and results obtained in ORSB free from obvious failure; the effects become large near $T = 0$ and better approximations are required. Yet the ORSB-approximation has the virtue to predict correctly the existence of a transition and to provide crude analytical solutions (without too many integrals). Moreover, RSB has the power to generate nontrivial critical behaviour in the range-free model; mean field critical behaviour only refers to the elimination of critical fluctuations in real space. We shall see this further below from the 4RSB-results of section V III.

We conclude this section with a demonstration of the typical difference between band asymmetries generated by ferromagnetic order (assuming here a model with nonvanishing ferromagnetic mean interaction $hJ_i > 0$ and $U = 0$, Figure 3 (left)) and the effects of the Hubbard interaction with $U > 0$ while $hJ_i = 0$ in Fig. 3 (right). We chose a strong doping case with a pronounced central band. The spin glass gaps are present in both cases. Ferromagnetic order shifts spectral weight from the upper magnetic band into the lower one and simultaneously renders the nonmagnetic central band asymmetric as well. On the right side the asymmetry above freezing is only due to the deviation from half-filling, which below T_f becomes accentuated by the spin glass gap at β , which splits off the central band from the upper magnetic band.

Figure 3 appended (g3.jpg) at e.o.f.

FIG. 3. Comparison of strong band asymmetry effects induced either by partially ferromagnetic interaction (left) with $hJ_{ij} = 1.5$; $\beta = 0.7$; $U = 0$ and self-consistent ferromagnetic order or (right Figure) due to a large chemical potential $\mu = 5$ with Hubbard coupling $U = 4.4$ and $hJ_{ij} = 0$ above half-filling. In the latter case the lower spin glass gap is immersed in a large Hubbard gap and the upper spin glass gap hosts the Fermi level, while in the left Figure only spin glass gaps, symmetrically placed with respect to $E = 0$, are excavated in the presence of strong additional ferromagnetic order. The high temperature regime of the right hand side Figure shows two energy levels with Hubbard splitting in the clean atomic limit; the random magnetic interaction with variance J (set equal to 1) distributes their weight into bands which remain well separated for the chosen ratio $U = 4.4$.

V. SOLUTIONS WITH 1-STEP REPLICASYMMETRY BREAKING

Since RSB-effects are strongest in the low temperature regime, we show first the 1RSB results of all relevant physical parameters of our present $J-U$ model (1) in the range between $T = 0$ and moderate temperatures $T = 0.25(J)$. These are collected in Fig. 4. For $T = 0$ the self-consistency equations show that the $(T = 0; U = 0)$ -solution can be used to find the $(T = 0; U > 0)$ solutions simply by applying the shift $\epsilon \rightarrow \epsilon + U$. This relation can be concluded from the exponential divergence $e^{-(U+\epsilon^2)}$ (in case that $\epsilon > U=2$) of expression (17) as $\epsilon \rightarrow 1$ and, of course, is confirmed by our numerical evaluations.

Figure 4 (g4.jpg) appended at e.o.f.

FIG. 4. 1RSB-solutions are shown for fixed Hubbard-coupling $U = 0.5J$ in the chemical potential range from particle-hole symmetry, $\mu = U/2$, to almost the discontinuous breakdown of the magnetic phase at $\mu = 1/4$, and in the temperature-interval $0 \leq T \leq \frac{1}{4}$: the T-normalized Parisi parameter $a(\mu; T) = m(\mu; T)/T$, the order parameters $q_1(\mu; T)$, $q_2(\mu; T)$ and their difference, the equilibrium susceptibility $\chi(\mu; T)$ and single valley susceptibility $\chi_s(\mu; T)$. Traces of the nonanalytic behaviour caused by the half-filling transition at $(\mu = U/2; T = 0)$ disappear with increasing temperature.

Using these solutions we obtain the density of states. Characteristic cases are displayed in Fig 5. On the left $\rho(E; T)$ for $\mu = 1; U = 0.5$ demonstrates for large filling how the broader Hubbard-SG gap and the upper SG-gap are filled by thermal excitations. The right Figure $\rho(E; T)$ shows a clear cut nonmagnetic central band together with a visible combination of gap widths at the very low temperature $T = 0.01$ and $U = \frac{1}{2}$.

Figure 5 (g5.jpg) appended at e.o.f.

FIG. 5. Density of states $\rho(E = \mu + i\eta; T)$ for $\mu = 1; U = \frac{1}{2}$ (left Figure) showing thermal smearing of Hubbard- and spin glass gaps and (in the right Figure) weakly thermalized gaps in $\rho(E; T)$ for $T = 0.01; U = \frac{1}{2}$ (all energies in units of J). The position of the Fermi level is indicated by a thick line, showing the crossover from a spin glass gap into the combined Hubbard- and spin glass gap. Both figures are obtained in 1RSB-approximation.

The symmetry between lower and upper magnetic band demonstrate that the half-filling transition coincides with the disappearance of the central band as the chemical potential falls below the critical value. As a guide to the eye a thick line shows the position of the Fermi level, which leaves the SG-gap below a critical (U) and moves deeper into the Hubbard regime as $U =$ further increases. The presence of a central nonmagnetic band is synonymous with a deviation from half-filling in this model. It exists for chemical potentials within the interval $\mu_k < \mu < \mu_c$, where $\mu_k \neq 0$ for $k = 1$ steps of RSB and μ_c denotes the threshold value for the spin glass phase.

VI. HALF FILLING PHASE TRANSITION AT $T = 0$: EFFECT OF THE COMPETITION BETWEEN HUBBARD REPULSION AND CHEMICAL POTENTIAL

A. Splitting and recombination of gaps

The half-filling transition is sharply defined at $T = 0$. We summarize the superposition and splitting of Hubbard- and spin glass gap(s) in the following Figure 6. The spin glass gap (note in ORSB) turns into a pseudogap at the Fermi level in the exact solution, since RSB splits spectral weight into the bright/vacant regions exempting only the Hubbard gap (blue) and the pseudogap line along $E = E_F$. Thus Figure 6 exhibits a change between two very different insulating phases: in the first phase, for $\mu > U$, the Hubbard interaction has effects only remote from the Fermi level, while in the half-filled regime ($\mu < U$) the Fermi level changes over into the Hubbard gap regime.

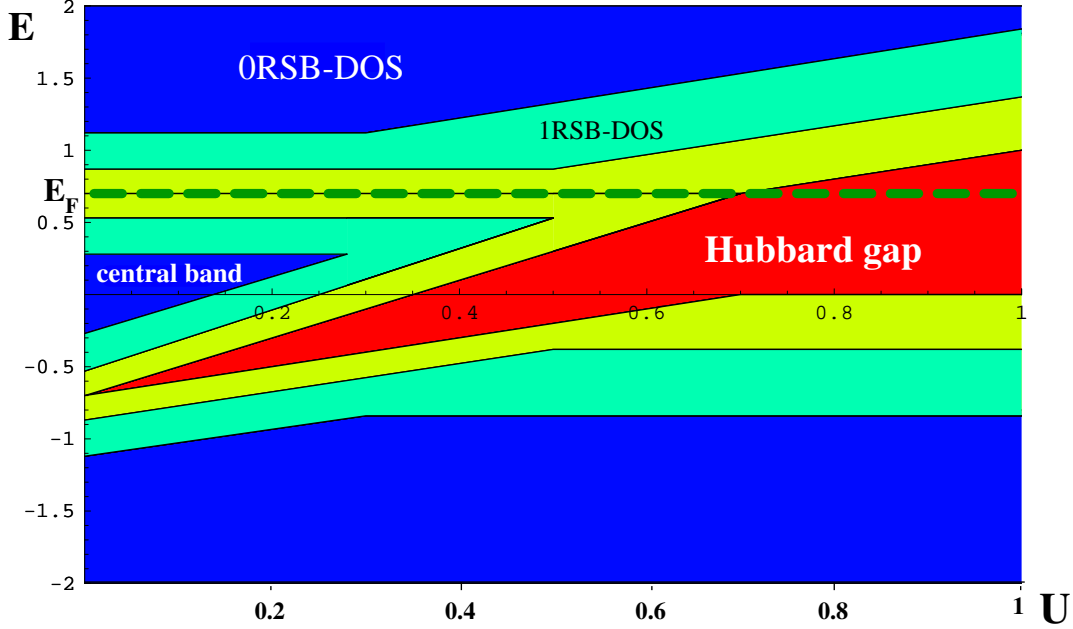


FIG. 6. This Figure illustrates the crossover (along the dashed line) of the Fermi level between different gaps in the $E; U$ -plane at $T = 0$. Dark grey regions show nonvanishing density of states in 0RSB-approximation, light grey the extension of these domains in 1RSB. The DOS-landscape is viewed from above. For a chosen $E_F = 0.7$ in the example shown, E_F pins the upper spin glass gap for $U < 0.5$ and moves into the Hubbard gap for $U > 0.5$. At $T = 0$ the central nonmagnetic band becomes fully suppressed for any Hubbard repulsion stronger than $U = 2$, which then implies half filling. In the exact solution the gap region is reduced and consists of Hubbard gap and spin glass pseudogap (of zero width).

The way in which 2RSB and higher corrections fill vacant regions of Figure 6 with small but finite spectral weight becomes obvious from the results of our paper. Here we want to avoid information overflow in the Figure. For the same reason, small deviations from straight lines are not shown, which occur beyond half filling (but, as found below in the paper) are identified as RSB-artifacts. The exact solution really realizes $\rho(E) = 0$ only along the straight line at E_F and in the Hubbard gap region. The transition between two different types of insulating phases remains as described by Figure 6.

Another type of soft filling into the regions, where Figure 6 still shows evacuated spectral weight, occurs due to thermal effects. The transition between Hubbard/spin glass gap phase into the pure spin glass gap phase will be manifested for example in the specific heat (as usual specific heat results are reasonable down to temperatures of the order $T > T_k \sim E_{gk}$, where E_{gk} denotes the gap energy in kRSB).

In which way transport processes will scatter weight into the gap regions is a matter of speculation for the moment. Essential parts of the present paper are however concerned with a sufficiently good determination of the fermion propagators for the insulating phase, which then provide the means to analyze transport effects in a perturbation theory.

VII. DEPENDENCE OF ORDER PARAMETER, SUSCEPTIBILITIES, AND FILLING FACTOR ON THE CHEMICAL POTENTIAL: A 2RSB-ANALYSIS AT ZERO TEMPERATURE

The half filling transition requires a more refined analysis of replica symmetry breaking effects. The dependence on the chemical potential is therefore calculated in a selfconsistent 2RSB-approximation for the full range of μ for which the spin glass phase exists. We determine all relevant parameters in this section, distinguish RSB-artifacts from true μ -dependence, and in particular determine the ν which helps to change arbitrarily between dependence on filling (fermion concentration) or on chemical potential. The filling factor is also linked to the integrated density of states (provides internal consistency check), which is determined in greater detail later in the paper.

A . Analytical input for the numerical solution at $T = 0$

The extremization of the free energy at finite temperatures is too complicated to have yet led to an analytical solution. The $T = 0$ -limit however allows one to reduce the number of integrations. This facilitates a low T -expansion and eases the numerical evaluation. We take advantage of this simplification and derive the complete set of $T = 0$ quantities. The $T \rightarrow 0$ -limit leads to the following energy $F(0)$ (per site and in units of J) which, unlike the thermal $F(T)$, depends on three (instead of four) order parameters $q_{1,2,3}$, two Parisi parameters $a_{2,3}$ and $m_{2,3} = T$, and the so-called single valley susceptibility. Extremizing

$$F(T = 0) = \frac{1}{2} (q_1 - 1) + \frac{1}{4} a_1 (q_1^2 - q_2^2) + \frac{1}{4} a_2 (q_2^2 - q_3^2) - \frac{1}{a_2} \int_{z_3}^{z_G} \ln \int_{z_2}^{z_G} C_0(z_2; z_3) \quad (32)$$

where

$$C_0(z_2; z_3) = \frac{1}{2} \int_{-1}^X e^{a_1 (H_{eff}(0;0;z_2;z_3) + a_1 (q_1 - q_2) = 2)} f_1 \operatorname{erf} \left(\frac{H_{eff}(0;0;z_2;z_3) - a_1 (q_1 - q_2)}{2 (q_1 - q_2)} \right) g \\ + \frac{1}{2} e^{a_1 (q_1 - q_2) = 2} \operatorname{erf} \left(\frac{H_{eff}(0;0;z_2;z_3)}{2 (q_1 - q_2)} \right); \quad U = 2 \quad (33)$$

with $H_{eff}(0;0;z_2;z_3) = \int_{q_2}^p \frac{1}{q_3} dz_2 + \int_{q_3}^p \frac{1}{q_3} dz_3$ leads to six coupled (double-)integral equations

$$f @_{a_1}; @_{a_2}; @_{q_1}; @_{q_2}; @_{q_3}; @_g F(0) = 0 \quad (34)$$

where $@_x$ means $\frac{\partial}{\partial x}$ (Eq.32 holds for the $U=2$ 0-side particle hole symmetry and up to irrelevant constants). We determine numerically all parameters for $U=0$ from the $T = 0$ selfconsistency equations which result from Eq.34. The results for $U = 0$ and half-filling are shown in the Figures below and all finite- U results can be obtained from it by the transformation $q \rightarrow q + U$ for positive U . We shall use the 2RSB-solutions to sort out artifacts of the approximation and understand the true underlying physics.

Figs.7 and 8 display new singular features in 2RSB which, by the help of a comparison with the 0- and 1RSB-results, can be suspected to be artifacts of the approximations; they nevertheless provide an improved insight into the shape of the exact Parisi solution in 1RSB. The analytic $T = 0$ -equations explain the origin of k-wiggles for k-stepped RSB. The surprising appearance of singular wiggles at smaller U involves multi-valued solutions and, similarly to what happens in first order phase transitions, would imply discontinuous behaviour. Finally one arrives at the conclusion that the wiggly behaviour must be associated with - and in fact is caused by - the stepped approximation of the continuous Parisi function in replica space. A physical meaning of these solutions could yet remain due to the fact that the 1RSB equilibrium solution is approached very slowly in time: finite-step RSB-solutions marked by the single- and two-valley susceptibilities might be relevant for non-equilibrium behaviour.

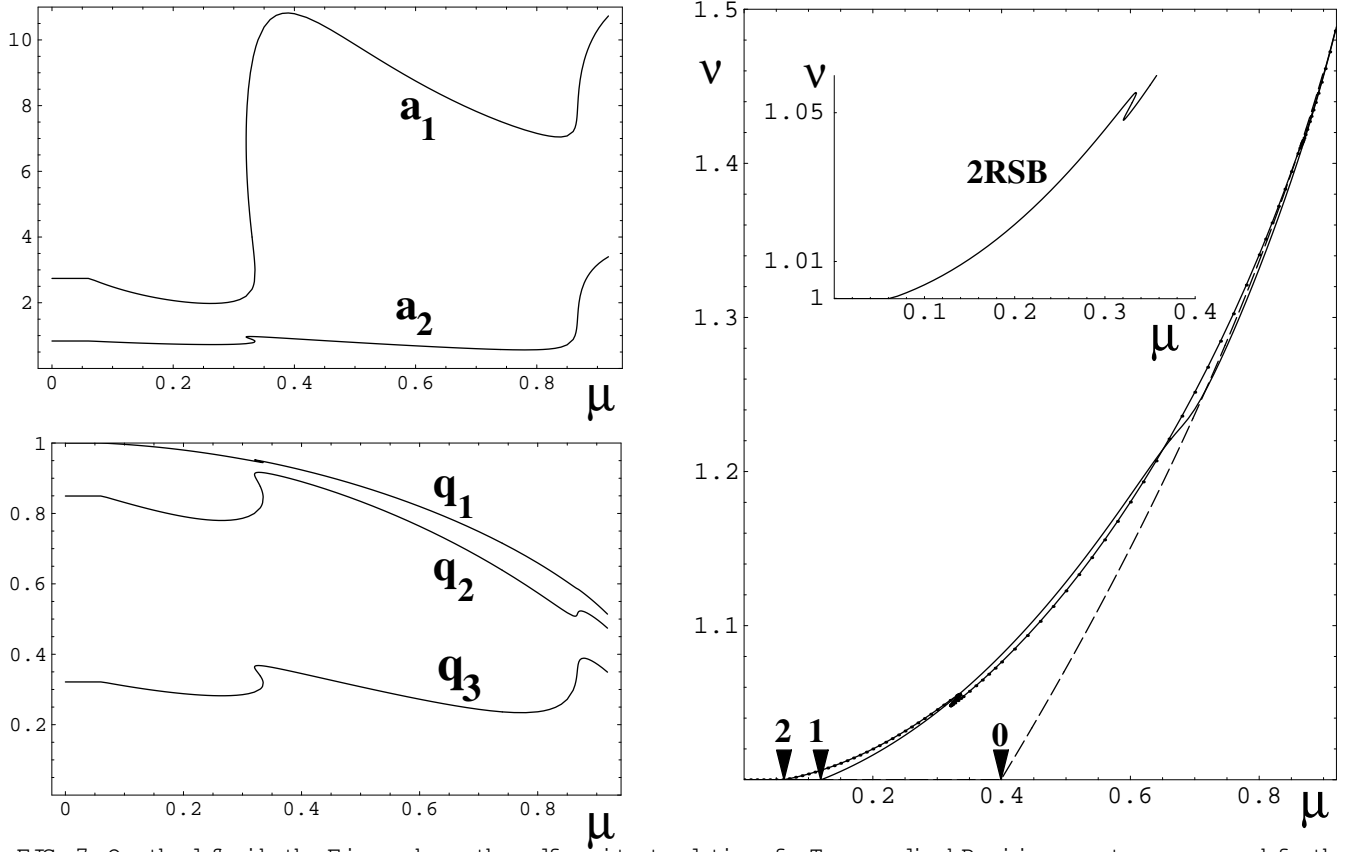


FIG. 7. On the left side the Figure shows the self-consistent solutions for T-normalized Parisi parameters $a_1; a_2$ and for the order parameters $q_1; q_2; q_3$ ($q=1$ not shown) at 2RSB-level as a function of the chemical potential μ ; on the right the fermion ionizing factor v is displayed, where labeled arrow-heads indicate the order of the approximation and the gap-size related limits of the half-lling regime at $j < (k=0;1;2)$ ($\mu=2$). The small region of a multi-valued ionizing factor is zoomed in the inset.

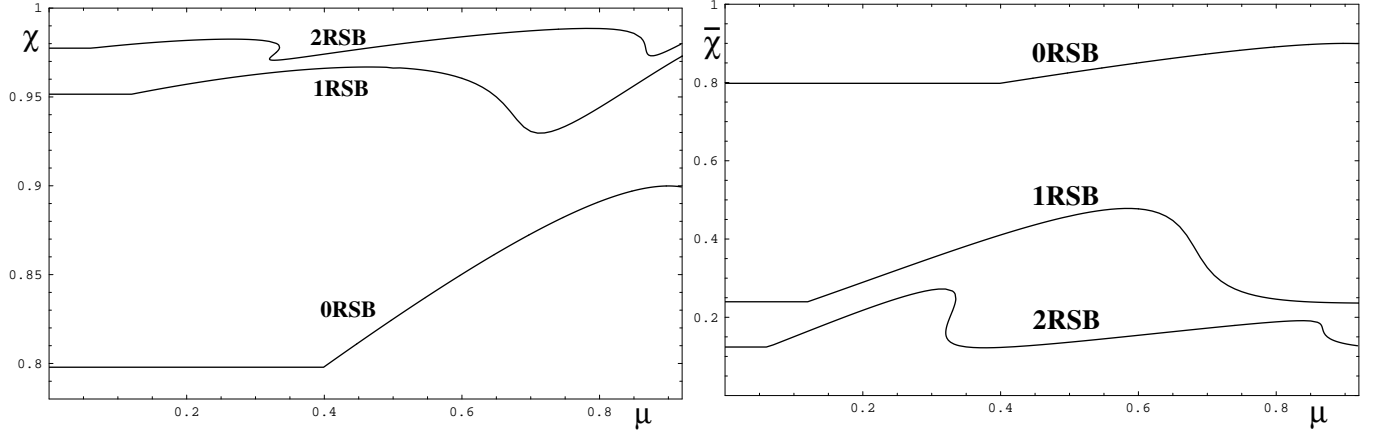


FIG. 8. The equilibrium susceptibility χ and single-valley susceptibility $\bar{\chi}$ are shown in 0RSB, 1RSB, and 2RSB approximation at zero temperature. The constant parts extend over the half-lling regime (at $T=0$) up to μ_{hf} given by $\mu=2$.

This discontinuous behaviour will be removed by thermal smearing in 2RSB down to much lower temperatures than observed in Fig. 4 or in the 1RSB-gap. The latter was seen to produce a smooth function like the expected exact solution. Throughout the paper we have chosen the chemical potential to be the independent variable. In order to see whether the μ -dependence is particularly susceptible to the soft steps, we inverted $v(\mu)$ into $\mu(v)$ and obtained the physical quantities as a function of the fermion concentration v as independent variable. It turns out that the wiggles seen in $v(\mu)$ itself do not remove (compensate) these features from the order parameters and susceptibilities

$q_1(\nu); q_2(\nu); q_3(\nu)$.

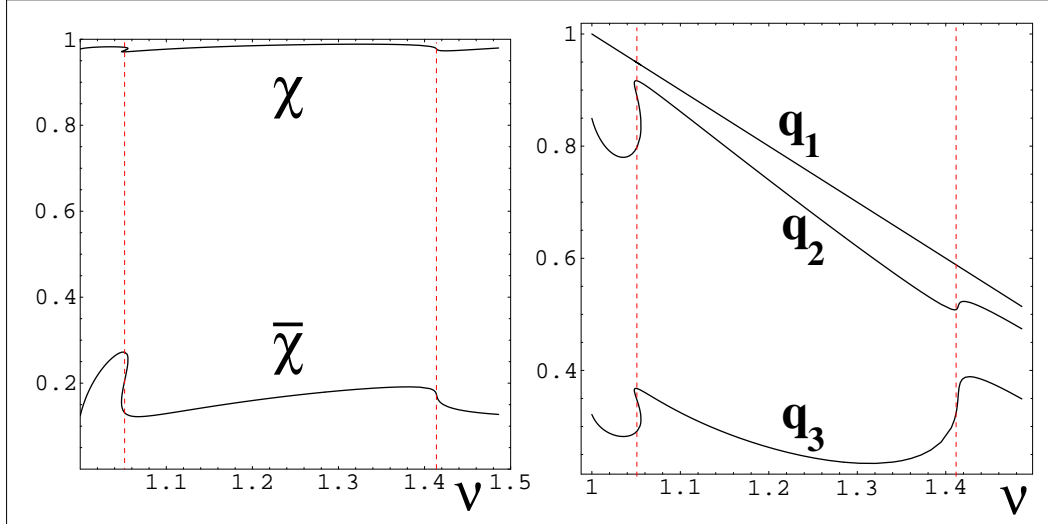


FIG. 9. Order parameters and susceptibilities as a function of fermion concentration ν in 2RSB-approximation. Vertical dotted lines locate wiggly behaviour generated by the Parisi steps in replica space.

Although some unphysical features are still contained in the $T = 0$ -solutions at any finite RSB, 2RSB-solutions are much closer to the exact ones.

Since the Parisi function $q(x)$ is constructed by piecewise continuous/constant functions of x (δ -functions below a break-point), the present results indicate that this dependence in replica space transforms either into strong variation or into jumps which resemble first order phase transitions. Their positions on the ν -axis scale with the step positions along the replica axis (replica dimension). A real discontinuous phase transition occurs however at the magnetic breakdown value 0.88 for $U = 0$ and shifted by U as shown in Figure 24. The critical filling is independent of the Hubbard coupling and roughly given by 1.45 .

By inspection of the selfconsistent equations one expects that the number of wiggles will increase with the number k of RSB-steps; the size of the jumps will diminish, thus improve the quality of the approximation, and finally disappear in the $k \rightarrow \infty$ -limit.

B. The order parameter as a function of chemical potential and $T = 0$ -measure of replica space

The 2RSB-results for the discretized order parameter and the intervals a_k of their step heights given in Figure 7 can be combined and represented in one Figure. An instructive representation of the generalized Parisi-function then results in the space of ν and of a variable called a_x . The latter replaces the variable x used by Parisi to represent the solution $q(x)$. In Parisi's papers, the continuous parameter x was introduced to host all matrix block size parameters m_k . These are found within an interval $0 \leq x \leq 1$ in the replica limit (in addition they lie dense in the 1RSB limit). The function $q(x)$ is discretized by means of δ -function (steps) in any finite order of RSB. In case of the low temperature limit, the selfconsistent solutions for matrix block size parameter m_k turned out to vanish linearly with temperature, which required the use of a rescaled parameter $a_k = m_k/T$. These parameter values are now hosted in an unbounded interval and we consider them as discrete values on an a_x -axis, where a_x replaces the low temperature limit of $x=T$ in a $T = 0$ calculation. Without temperature-rescaling the x -interval below the break point, where the nontrivial part of the Parisi function shows up, would collapse to a point with $q(0)$ infinitely-valued. The nontrivial part of the Parisi function still exists at $T = 0$ and is well represented on the a_x -axis. As a function of a_x and of the chemical potential we obtain the 2RSB-result of $q(a_x; \mu; T = 0)$ as given by Fig. 10

Figures 10 and 11 appended (g10-11.jpg) at e.o.f.

FIG. 10. 2RSB-approximation of the $T = 0$ Parisi order parameter as a function of $a_x = x/T$ $\lim_{T \rightarrow 0} m(T) = T$ and μ . The strongly μ -dependent interval lengths over which the order parameter assumes one of its possible three constant values are shown at the $\mu = 0$ -side of the plot. At the large $\mu = 0.88$ -side the first order regime of magnetic breakdown is shown.

FIG. 11. The calculated $T = 0$ limit of the free energy in 2RSB. For $U = 2$ the half-filling energy is higher (dashed line). The inset shows the multi-valued regime indicated by an arrow in the large-scale energy.

At $T = 0$ it seems possible that the solutions as a function of μ for very high k (close to the exact one at $k = 1$) will be made up of piecewise continuous functions of μ , where discontinuities at the $O(k)$ wiggles and the intervals of continuous behaviour both approach zero. Some resemblance with level crossing/repulsion appears. The wiggles must naturally be seen to mark a soft stepping of the order parameter in contrast to (and as a consequence of) the hard steps along which are imposed by the definition of the Parisi scheme. One may be tempted to ask for a generalized scheme that softens the steps also in the replica dimension before the exact limit is reached. This seems even more desirable since the higher order RSB-calculations below show an extreme flatness of the energy landscape. Using the above solutions we calculate the $T = 0$ -limit of the free energy of Eq.(32). The solution shown in Fig.11 confirms the half-filling limit at $\mu = 0$ and a discontinuous transition near $\mu \approx 0.33$. Thus it is clear that the step-approximation of the order parameter function in replica space leads either to strong variation or to jumps, which appear in the form of artificial first order transitions at certain values of the chemical potential; these locations correspond to and scale with the positions of the Parisi-steps. No such transition can be expected in the exact solution. One could speculate whether $\mu = 0$ is the accumulation point of these discontinuities and thus may be the source of special critical behaviour in the $\mu = 0$ point in 1RSB. In this case infinitely many wiggles could render the Parisi function a mathematically delicate object at half-filling. While Parisi's finite temperature order parameter function $q(x)$ is defined on an interval $0 \leq x \leq 1$ the present replica interval for $T = 0$ is unbounded and there is not yet an indication that the discontinuities must lie dense in the limit of infinitely many RSB-steps. The conclusion of this chapter is that the μ -dependence seen in the susceptibilities will disappear and yield $\chi = 1$; $\mu = 0$, while the order parameter function decreases smoothly as μ approaches the magnetic breakdown value and steps along the a_x -axis must be continued. In this sense Figure 10 offers a crude picture which calls for an improved and refined treatment. Before this is achieved in section VIII the fermion filling factor ν , which is related for $T = 0$ to the largest order parameter q_1 and also to the integrated density of states, is obtained.

C. The $\nu(\mu)$ -dependence from 2RSB-calculation for the whole spin glass regime

The spin glass regime exists at $T = 0$ in the range $0 \leq \mu \leq U/2$ for positive U . Comparing the kRSB-results for $k = 0;1;2;3;4$ together with the known exact value at $\mu = 0; T = 0$ the regime of validity and the quality of 2RSB can be estimated. An interpolation helps to conjecture the form of the expected exact solution $\nu(\mu)$. The numerical result can also be used to generate an analytical fit, which in the best case would be the exact solution. If not exact, it can still represent an analytical form for the propagator needed in diagram expansions of itinerant models for example. Figure 12 shows such an interpolation. The fermion concentration $\nu = \frac{1}{2} d \nu(\mu)$ at $T = 0$ equals $2 - q_1 = 2 - q_1^a$.

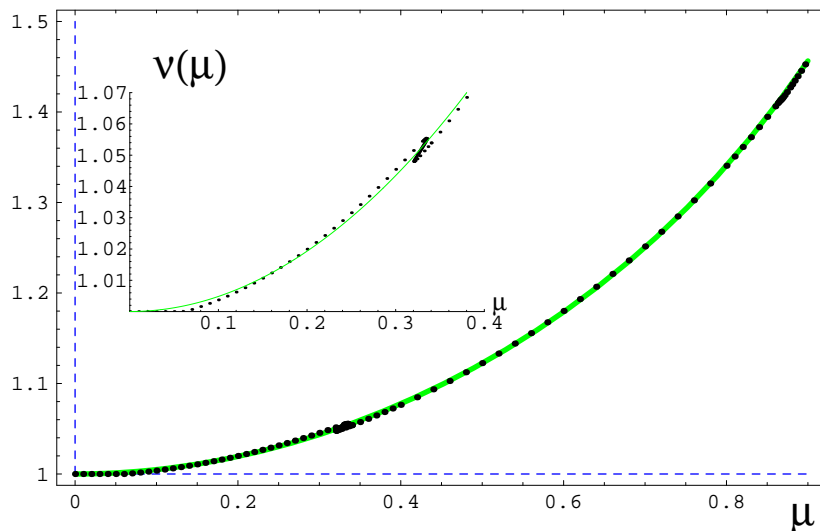


FIG. 12. The known exact value at half-filling is joined with the 2RSB-approximate values of the fermion filling factor as a function of the chemical potential. The RSB-artificial wiggles are almost innocuous on this scale.

Only the zoomed inset in Figure 12 shows significant deviations between the $\phi(\beta)$ t-function and the 2RSB-calculated points. Viewed more globally over the whole β -interval a simple quadratic behaviour with small quartic corrections fits nicely. The exact behaviour of $\phi(\beta)$ appears to be simple. The t function, which interpolates between $\phi_{\text{exact}}(\beta = 0) = 1$ and 2RSB-values for $\beta > 0.12$, is close to $1 + \frac{1}{2}\beta^2 + O(\beta^4)$. The way in which the finite half filling limits ($\beta = 1$) move to smaller chemical potentials is determined in the following section VIII, concerning the interpretation ².

VIII. THE SHAPE OF THE SPIN GLASS PSEUDO-GAP, ITS COMBINATION WITH THE HUBBARD GAP, AND A COMPARISON WITH THE EFROS-SHKLOVSKII COULOMB PSEUDOGAP : 4RSB-CALCULATION AT HALF FILLING , EXACT RELATIONS

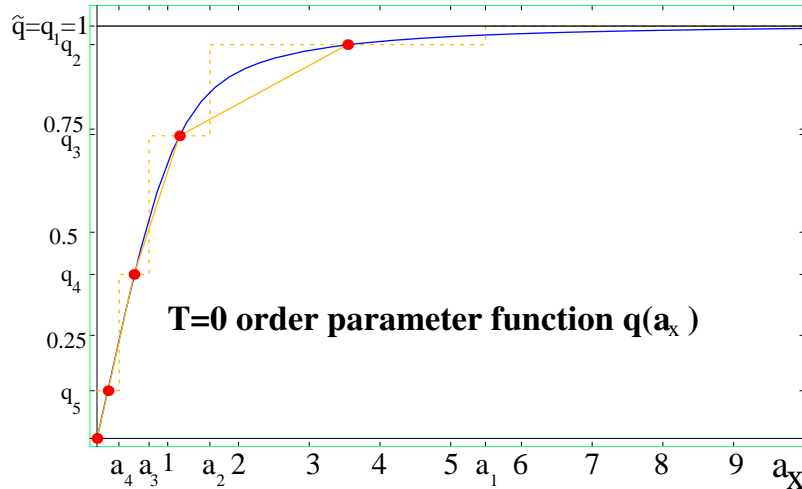
We extend the above-mentioned extremization of the free energy, Eq.34, to a 4RSB-solution. On this level and for arbitrary filling, the set of ten coupled integralequations, each having seven coupled integrations,

$$f_{a_1}; \phi_{a_2}; \phi_{a_3}; \phi_{a_4}; \phi_{q_1}; \phi_{q_2}; \phi_{q_3}; \phi_{q_4}; \phi_{q_5}; \phi_{gF}(0) = 0 \quad (35)$$

must be solved selfconsistently. We performed this calculation for half filling where the numerical efforts are reduced to the solution of eight coupled equations, since $q_1 = 1$ and the ϕ -equation decouples from the rest. If the points in replica space, where the order parameter values are sought, would not be required to minimize the free energy too one could include several higher RSB-orders with similar effort. This seems however unnecessary for the present purpose and hence was discarded.

A . 4-step RSB approximation for $T = 0$ -order parameter function and χ -susceptibilities at half filling

While a Parisi order parameter function for finite temperatures is defined on an interval $0 < x < 1$, the $T = 0$ order parameter function is represented by the temperature rescaled quantity $a_x = \lim_{T \rightarrow 0} x = T$, which is the natural choice due to the $m(T) \propto T$ dependence observed in our selfconsistent calculations. An upper bound for the selfconsistent a_x -solutions does not seem to exist. The maximum value in 4RSB is 5.5 and grows rapidly with the order of RSB. A mapping $a_x \rightarrow \tilde{a}_x = a_x/(1 + a_x)$ has the virtue of re-converting even the $T = 0$ interval to $0 \leq \tilde{a}_x \leq 1$. The following Figures show the obtained selfconsistent values and the fitting continuous order parameter function at $T = 0$. The fitting analytical form indicates that a distribution of error functions is probably involved in the exact analytical solution of the problem .



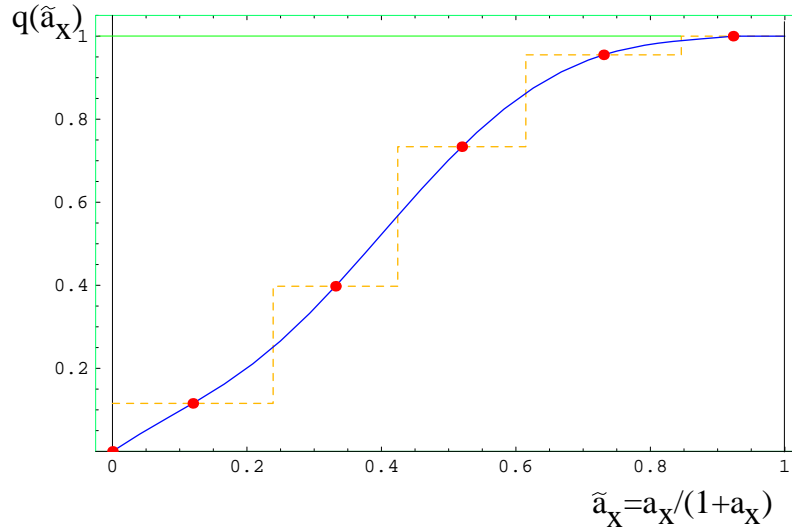


FIG. 13. A $T = 0$ order parameter (analytic model) function, which fits well the calculated 5-step (4RSB) approximation, is shown. The upper Figure displays $q = q_1 = 1; q_2; \dots; q_5$ and $fa_1; \dots; fa_4$, all obtained selfconsistently, for the original variable a_x . Below, the same function is shown as a function of a_x after mapping to the interval $[0;1]$ by means of $a_x \rightarrow a_x/(1+a_x)$.

A break point, which is a specific finite temperature Parisi order parameter function $q(x)$, appears to be absent in accordance with the expectation: the break point scales like $x_{BP} \propto 1/T$ and since $a_x \rightarrow x=T$ one expects this point to move to infinity in the zero temperature limit. The equilibrium and nonequilibrium susceptibilities, obtained from our 4RSB-calculation are shown in Figure 14. The χ -decay is well modeled by a function which decays like $1/k$ when the number of k RSB-steps goes to infinity. Logarithmic corrections or a slower decay cannot yet be ruled out.

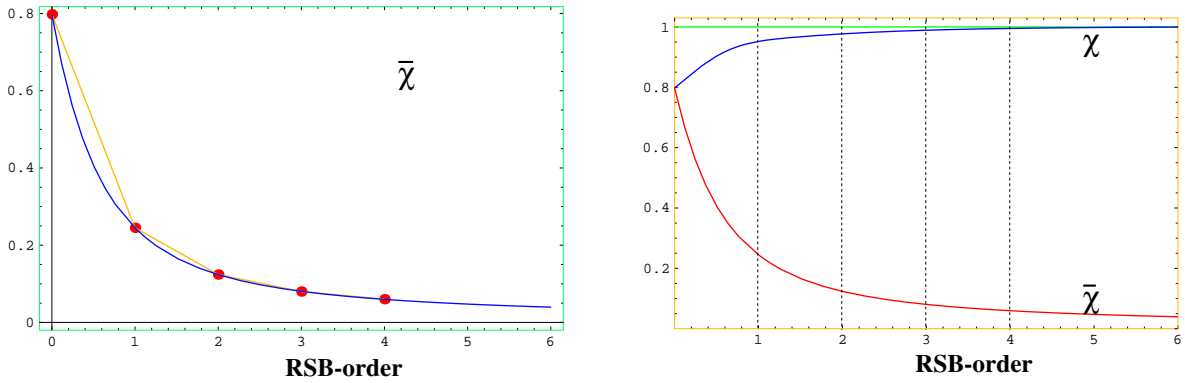


FIG. 14. The decay of the single-valley (nonequilibrium) susceptibility is shown as a function of interpolated RSB-order; calculated points are shown by dots and extrapolation to higher order is possible from a simple and good analytical model fit. The growth of the equilibrium susceptibility towards 1 is shown in comparison with the χ -fit in the Figure below.

B. 4RSB-approximation of the spin glass pseudogap

Thermal effects cover unphysical remainders of replica symmetry and, as one increases the order of RSB, the reappearance of incorrect features shifts to ever smaller temperatures. In a comparable way one needs higher orders of RSB to describe exactly smaller and smaller excitation energies above (and below) the Fermi level. In other words, $E - E_F$ scales with T and the larger the excitation energy is the smaller is the effect of the 'fine structure' of the Parisi function for small a_x as shown in Figure 13. The effect can be seen in the fermionic density of states at $T = 0$. It will also enter the quantum-dynamical fermion propagator, which is determined by its spectral weight. We improved earlier one-step RSB-calculations¹⁵ by three orders and found that four-step RSB (4RSB) is sufficient to predict the shape of the pseudogap.

We derive the exact 4RSB-formula for the fermionic density of states ($E > 0$) for $T = 0$ as

$$\rho(\epsilon) = e^{a_1(\epsilon)} \left(\frac{1}{2} \frac{1}{(q_1 - q_2)} \right)^{\frac{1}{2}} \frac{1}{N_2(a_4=a_3)} \frac{1}{N_2(1-a_4=a_3)} \frac{1}{N_1(1-a_3=a_2)} \frac{1}{N_2} e^{(\epsilon - H_{eff})^2 = (2(q_1 - q_2))} C^{a_2=a_1-1} \quad (36)$$

using the integral operator $R_b = \int_{z_b}^R \frac{R_G}{z_b} \frac{R_1}{1} dz_b \exp(-z_b^2/2) = \frac{1}{2}$ acting on the accumulated normalizing factors

$$fN_1(x) = \frac{1}{2^0} C^{a_2=a_1} x; \quad N_2(x) = \frac{1}{3^0} \frac{1}{2^0} C^{a_2=a_1} x \quad (37)$$

and C as given by Eq.33 after replacement of the 2RSB by the 4RSB-effective field H_{eff} . Our numerical evaluation of Eq.36 for half-filling and $U = 0$ is shown in Fig.15.

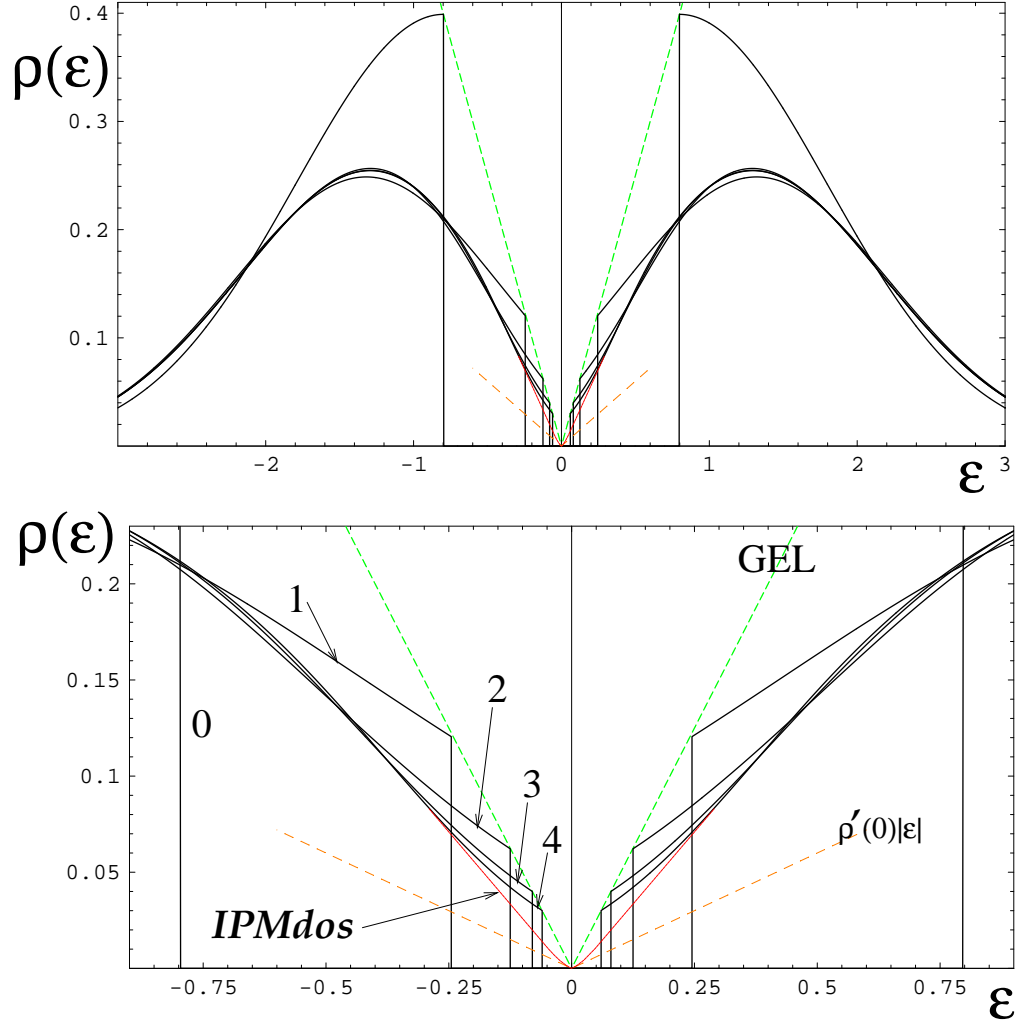


FIG. 15. The magnetic band structure at $T = 0$ and for half-filling is shown for comparison in the replica-symmetric (0RSB), 1-, 2-, 3-, and 4-step replica symmetry breaking approximation (solid curves labeled with 0;1;2;3;4 correspondingly). The gap energies decrease with the increasing RSB-order and the shape of the gap emerges. The wide scale upper Figure shows the decrease of width and position of energy regimes, where the next higher order of RSB bifurcates. The bottom Figure zooms the gap regime near E_F . The dashed gap-edge-line 'GEL' shows the exact lines connecting (E_g) (E_g denoting the gap edge energies) while the asymptotic power law in the limit $\epsilon = 0$ is indicated by the dashed line $\rho'(0)|\epsilon|$ with $\rho'(0)$ approximated by its 4RSB-value 0.13. An interpolation IPMdos of the density of states between the tiny gap-bottom regime following this law and the wide gap regime (where 4RSB is almost exact) with a slope closer to 0.3 is modeled by extrapolating a $\rho(0)$ -calculation to 1 RSB.

The dash-dotted straight lines locate the shoulder-height ($E_{g;k}$) at the gap edges $E_{g;k}$ of k -step RSB : the ratio between these heights and the gap-width is invariant ($= 1$) under a change of the order k of RSB, is RSB-invariant.

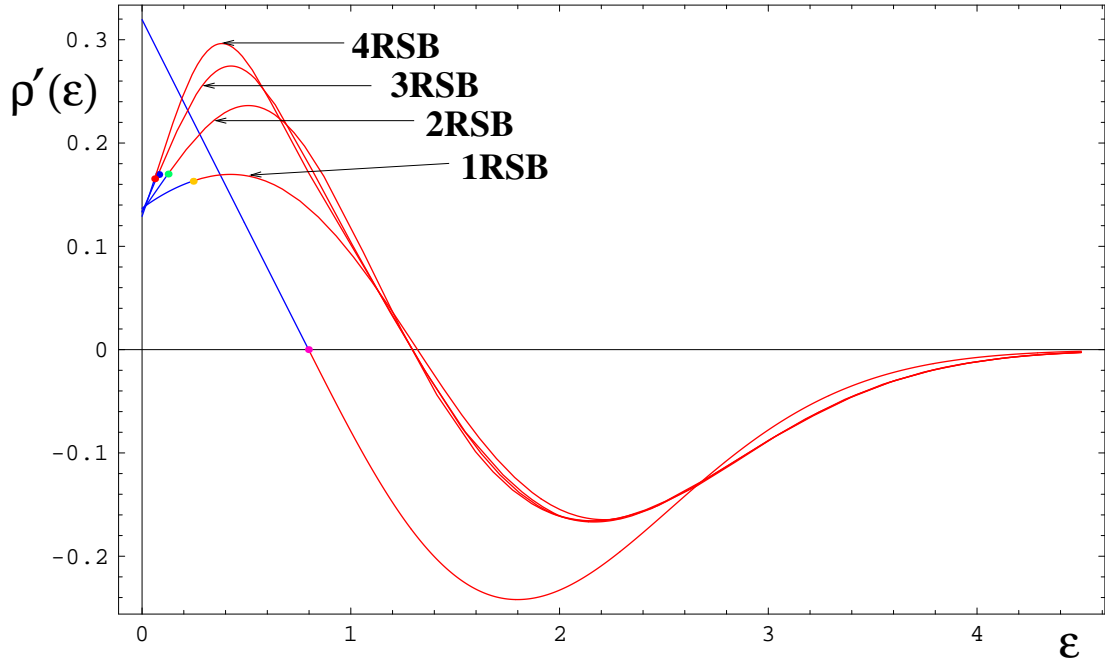


FIG .16. First derivative of the density of states (ρ'), $E \in \mathbb{R}$ from replica-symmetric to four-step RSB approximation. Gap edges are indicated by points for each approximation and an extrapolation beyond these points towards the Fermi level ($\epsilon = 0$) is shown. These lines demonstrate the rapid convergence: lines from 2 ; 3 ; and 4RSB lines meet in the point $(0; 0.13 + O(10^{-3}))$.

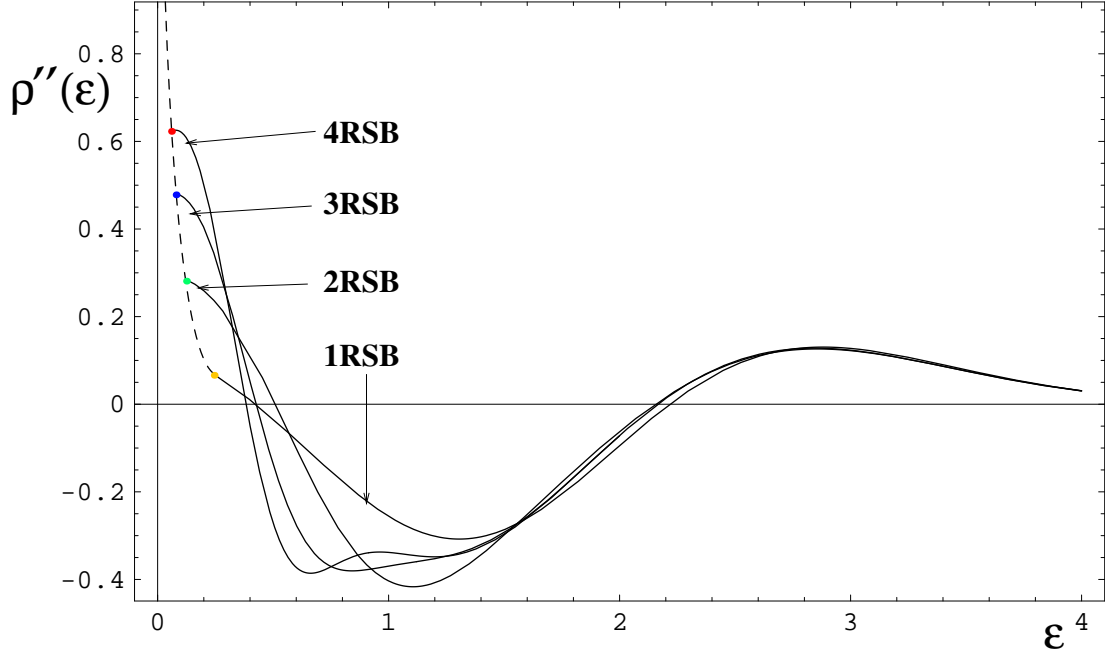


FIG .17. The second derivatives of the density of states does not show rapid convergence up to fourth order replica symmetry breaking. Dots mark again the gap edge positions $\epsilon = E_{g;k}$ in k -th order RSB. Their position is well fitted to the shown curve (dashed) $\rho''(E_{g;k}) = 2.1 - 7.9 E_{g;k} + 7.6 E_{g;k}^2$. This serves as a crude estimation of $\rho''(0)$ in 1RSB. A divergence of $\rho''(0)$ can however not be excluded, which would imply the subleading exponent of $\rho(\epsilon)$ to be smaller than 2.

In Figure 16 the gap edge points E_{gk} must reach $= 0$ in the 1 RSB limit; whether these values E_{gk} for further increasing values of k eventually fall on a curve with divergent slope for $\neq 0$ can not yet be concluded from Figure 17. This affects only the subleading behaviour which determines the curvature within the very small asymptotic scaling regime. Figure 18 illustrates the remaining small corrections beyond 4RSB . The interpolating approximation to the exact solution shows the smallness of the scaling regime, while the larger linear regime up to ≈ 1 can be viewed as subcritical. Without a closer look it is hardly possible to see that the extrapolation of the almost linear DOS-decay would not end in $= 0$ but leave a tiny finite fake-gap. This is prevented by the crossover to the scaling regime as described in the zoomed part of Figure 15.

Figure 18 (g18.gif) appended at e.o.f.

FIG. 18. The magnetic band structure at $T = 0$, for $U = 0$, and half-filling. The 4RSB -approximation, which contains only a tiny gap, is shown in comparison with the interpolated model (IPM dos) of full RSB matching $(E_F) = 0$ and the $^0(E_F)$ j-law, concluded from RSB -convergence towards $^0(E_F) \approx 0.13$ of Figure 16, with the regime $j > 0.3$ where the 4RSB -values are effectively exact.

Effects of the Hubbard interaction: At zero temperature and for half-filling the effect of the Hubbard coupling is to spread the spin glass gap by the U and to shift the symmetry point $\rightarrow U=2$. The repulsive Hubbard interaction preserves half-filling and maintains the gap even in the limit of 1RSB .

Figure 19 (g19.gif) appended at e.o.f.

FIG. 19. The density of states for vanishing Hubbard interaction and asymptotic j -behaviour is shown in comparison with one for finite Hubbard repulsion $U=J=1$. At $T=0$ and for half-filling the Hubbard gap splits the spin glass pseudogap in two halves and preserves the form of the linear γ -decay relative to the gap.

It is perhaps unexpected to evoke universal critical behaviour in the context of a pseudogap in a range-free (or in finite-dimensional) model. However the results indicate that critical correlation equivalents appear to exist in replica space. It is in this space that a theory perhaps of renormalization group character should be developed in order to analyze the critical behaviour (shape) of the pseudogap. In the better known case of finite range interactions (in finite dimensions) the renormalization group approach as defined and applied to the Coulomb pseudo-gap by Johnson and Kholmitski²⁹ is a related very interesting but low-dimensional example. Renormalization group studies of random magnets of Ref. 30 and techniques described in the review by Shankar³¹ must be considered to eventually understand the spin glass gap in presence of long-range Coulomb interaction too.

C. Fermion propagator and spectral representation

Perturbation expansions, which use the present model as a free (solvable) limit, are an interesting possibility to study for example itinerant spin glass models. In such expansions the fermion propagator, which is a site-localized propagator in time, should be known analytically. In particular its analytical properties are required in order to be able to evaluate diagrams of the perturbation theory. While it is not yet clear whether an exact analytical solution can be found in the 1RSB -limit, the present analysis allows to approach this solution in a qualitative way. The numerical study helps to find an analytical t -function, which could be considered as a diagrammatic element in the expansions mentioned above. Using our previous result for the density of states $\rho(\omega) = \frac{1}{\pi} \text{Im} (G^R(\omega))$ the spectral representation

$$G(z_n) = \int_{-1}^1 \frac{du}{z_n - u} \quad (u) = (iz_n - u) \quad (38)$$

with $z_n = (2n+1)k_B T/\hbar$ allows to evaluate the real part and thus the full Green function too.

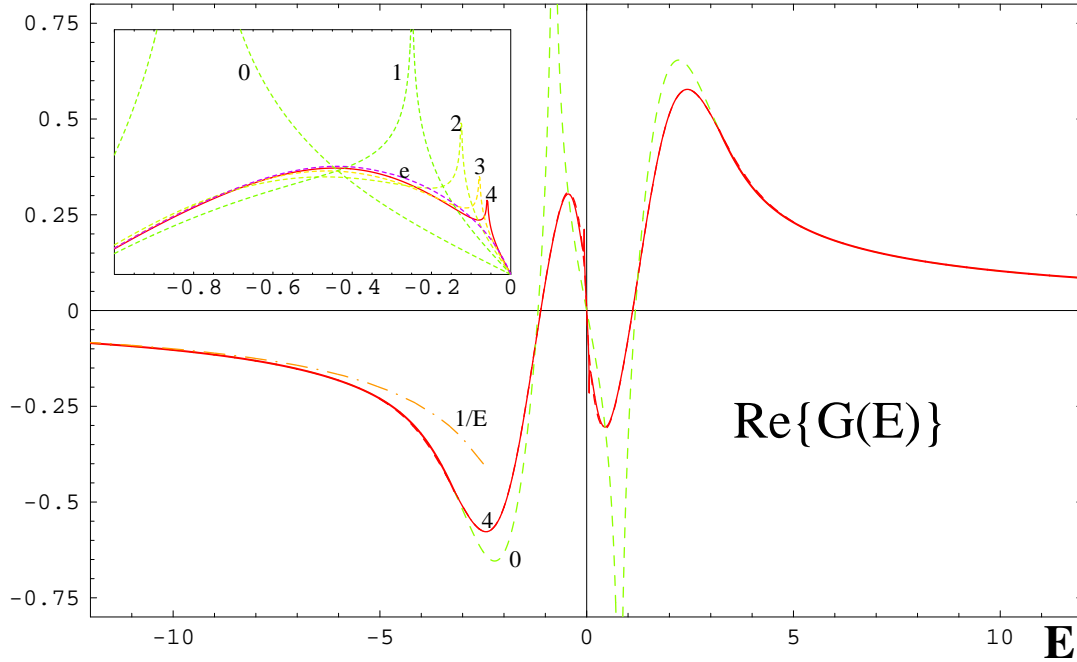


FIG. 20. The real part of the fermion Green function is shown for 0- and 4RSB over a wide energy range. The zoomed region (upper left inset) shows all calculated RSB -orders (0;1;2;3;4). The result from Eq.38 using the 1 RSB-DOS model is contained (dashed curve carrying label e) and visibly different from 4RSB only in the zoomed inset. Gap edge singularities (spikes) with positions depending on RSB -order k are observed; curves are labeled by the order k . The logarithmic gap edge singularities are cut off in numerical calculations by small imaginary parts $\epsilon = 0.10^{-6}$ in $E + i\epsilon$ which ensure a finite distance from the branch cut of G . The free $1/E$ -behaviour is shown for comparison.

Figure 20 (inset) shows the step-by-step approach of the exact solution. The limit of spin glass interaction effects is shown by the crossover into the free limit $1/E$; together with this one observes an energy range where even the replica symmetric approximation is almost exact (roughly for $|E| > 3$). The inset shows the increase in length of the well-approximated energy regimes with the growing order of RSB. The Figure also confirms the existence of hierarchical excitation energy regimes, where a certain minimal order of RSB guarantees an almost exact result. Moreover these regimes appear to scale with corresponding characteristic temperature regimes. We further observe that the logarithmic divergence of $\text{Re}(G)$ at the Fermi level appears to be compatible for the scale chosen for the main Figure; in the zoomed inset the slope at E_F looks finite even in the interpolation model. This model however includes the logarithmic divergence which emerges only in an exponentially small (invisible) energy range near the Fermi level.

The analytical result in 0RSB for the retarded fermion Green function for $T = 0$ and half-filling reads

$$G^R(E) = \frac{1}{8} \sum_{\alpha=0}^{\infty} \exp\left(-\frac{1}{2}c_{\alpha,E}^2\right) (0; c_{\alpha,E}^2) - i \exp\left(-\frac{1}{2}c_{\alpha,E}^2\right) (1 - \text{erf}(ic_{\alpha,E})) \quad (39)$$

where $c_{\alpha,E} = E + \alpha + i0_+$. The ϵ -function in this expression reproduces the logarithmic singularities at the gap edge energies as seen in the numerical calculation above. Eq.39 crosses over into the free $1/E$ -behaviour for large energies and is almost exact beyond $|E| > 3$, i.e. for excitation energies more than four times beyond the spin glass temperature (recalling $J = 1$). From Eq.38 it is clear that whenever $\rho(u)$ drops to zero at a gap edge energy, the Cauchy principal value integral must diverge logarithmically. Only in the 1RSB limit is $\rho(u)$ no more discontinuous; it is even in u and no divergence occurs in $\text{Re}(G(0))$. For finite Hubbard interaction the gap is not closed, but the density of states decays at least with some power at the Hubbard gap edge, which again prevents a singularity in $\text{Re}(G)$. By means of the rapid convergence of RSB, the numerical analysis supports that the slope of $G(E)$ at $E = 0$ diverges. Only in case when the spectral density vanishes faster than linearly at $E = 0$ the slope would remain finite.

Figure 21 (g21.gif) appended at e.o.f.

FIG. 21. Part a) shows $\text{Re}(G(\epsilon))$, real, in 4RSB-approximation and superimposed the result obtained from the interpolation model for the exact density of states. Very good agreement is obtained. Both curves can hardly be distinguished except in the tiny regime near the small 4RSB-gap edge at $j = 0.06$, which is absent in the exact solution. Innocuous too, although present in the interpolating model solution in an exponentially small region near the Fermi level, is the logarithmically divergent slope of the real part of $G(\epsilon)$.

Part b) shows the effect of the Hubbard interaction for $U = 1$ (in units of J) in comparison with the $U = 0$ -result contained in part a). For $U = 1$ the slope of $\text{Re}(G)$ does no more diverge at the Fermi level. The Hubbard interaction squeezes a hard gap of size U into the spin glass pseudogap. The logarithmic divergence at the Fermi level is therefore removed for all finite U .

In Fig 21 part b) a solution for finite Hubbard interaction $U = 1$ is compared with the $U = 0$ case; we justify the use of the 1RSB-model by the very good agreement with the calculated 4RSB-curve (once the RSB-artifact at the gap edge is omitted). The density of states together with Fig 21 give a complete picture of the true (local) fermion propagator. Starting from the numerical data for arbitrary values of the Hubbard coupling (in units of the spin glass coupling J) we are ready to create, on the basis of computer algebra, objects that can be dealt with like standard Green functions and hence be used in diagram theories.

The numerical analysis is completed by Figure 22 for the purely imaginary Green function $G(i\epsilon)$. Figure 22 shows a spectacular convergence already in the available low orders of RSB. Specific singular features, observed in $G^R(E)$ for real energies E , are absent on the imaginary axis (of course they are hidden and almost innocuous in $G(i\epsilon)$). The absence of singularities on the imaginary energy axis gives rise to the speculation that an unexpected simple approximate form of the exact spin glass propagator may be good enough for calculations on the imaginary axis (leaving aside problems with the analytical continuation to real energies).

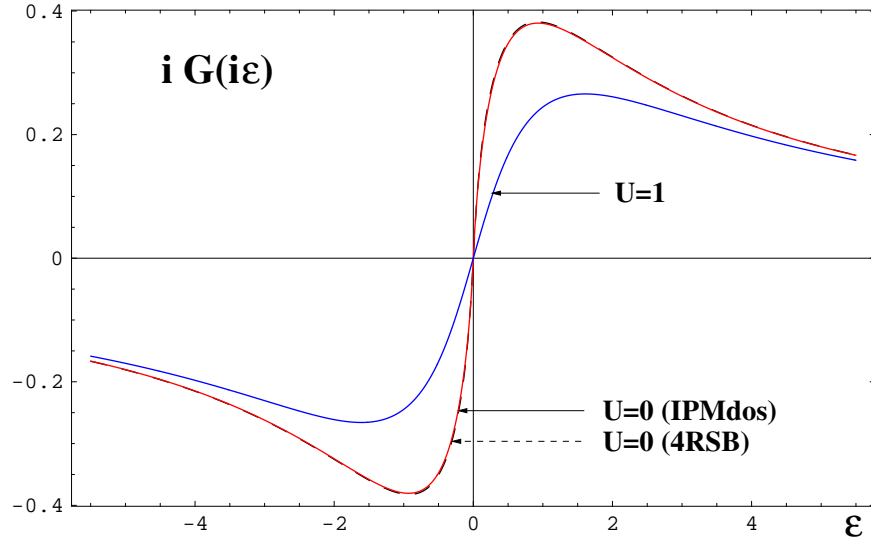


FIG. 22. The (imaginary) fermion propagator $G(i\epsilon)$ for half filling is displayed as a function of the fermionic frequencies $\epsilon_n = (2n+1)k_B T / \hbar$, $T \rightarrow 0$ which become continuous in the zero temperature limit. For $U = 0$, the dashed curve represents the 4RSB-calculated one, which almost perfectly coincides with the one calculated from the DOS-interpolation model for full RSB. The Hubbard interaction effect is shown for the chosen strength $U=J = 1$.

D. Scaling at the half-filling $T = 0$ -transition

The half-filling transition is sharp at $T = 0$ and becomes continuous as ϵ vanishes in the 1RSB-limit. It can be driven by the variation of either $\epsilon = E - E_F$ which controls the pseudogap-shape, or by $U - E_F$ which breaks down the central band. Finite temperatures act like a symmetry breaking perturbation which smears the transition. Our detailed RSB-calculations suggest the following scaling behaviour

$$G(\epsilon; T=0; \epsilon < U) \sim j^{-j} + A j^{-j} \quad \text{gap regime} \quad (40)$$

$$\frac{dG}{d\epsilon} \sim \ln j \quad \text{for } \epsilon \rightarrow 0 \quad (41)$$

$$1 - (U/\epsilon)^2 \sim 1 - q^{aa} = 1 - q_1 \quad \text{for } \epsilon > U \quad (42)$$

where Fig.12 suggests a subleading exponent $\gamma = 2$. Assuming that ρ scales like U near the transition one can propose the scaling form for the density of states

$$\rho(\epsilon; U; T) = A j^x f\left(\frac{U}{j}; \frac{T}{j}\right); \quad (43)$$

where, according to Eq.(40) our prediction is $x = 1$ for the infinite-range model, and f is meant to be the scaling function of the density of states.

For any finite k -step RSB the transition is discontinuous; viewing the influence of smaller and smaller order parameters q_k as $k \rightarrow 1$ as a disorder fluctuation effect reminds of conclusions stating that disorder fluctuations can render a transition continuous^{25,26}. The difference would be that we are concerned here with a one-dimensional defect in replica space, while those authors referred to real space fluctuations.

IX. A SCENARIO FOR THE SPIN GLASS DRIVEN METAL-INSULATOR TRANSITION

1. Non-half-filled system

According to the preceding chapters, a central band always exists if the system is not half-filled. Then, the Fermi level must lie inside the upper spin glass pseudogap, which is separated from the Hubbard gap by the central band. A metal-insulator transition must take place as fermion hopping increases beyond a critical value. Two possibilities arise: first the pseudogap defined by $\rho(E_F) = 0$ survives until the metal-insulator transition (MIT) takes place or, more likely, the pseudogap is gradually filled but states remain localized until the density of states becomes large enough. Then the MIT would take place. Its character must be different from standard Mott-Hubbard-Heisenberg metal-insulator transitions, since the gap's existence rests exclusively on the frustrated magnetic interaction and, in addition, the localization of states stems again only from the randomness of this interaction. No further random potentials or random scattering is necessary to localize states in a way similar to Anderson localization. We explained already in the introduction how the random magnetic order might act in this way. In this context one should recall that broken time reversal allows for the unitary type of Anderson localization. In this respect it is an interesting detail that spin glass order is a special breaker of time-reversal invariance TRI, since the random magnetic moments break TRI locally, but globally the magnetization is zero without field and a global average breaking is not present.

2. Half-filling

In the half-filled system all gaps combine into one. At $T = 0$ the spin glass gaps appear to be attached on each side of the Hubbard gap. The Fermi level lies in the center and one could expect the metal-insulator transition to be similar to that of the Hubbard model. However a detailed analysis must scrutinize this, in particular when the variance of the frustrated interaction is larger than the Hubbard coupling U .

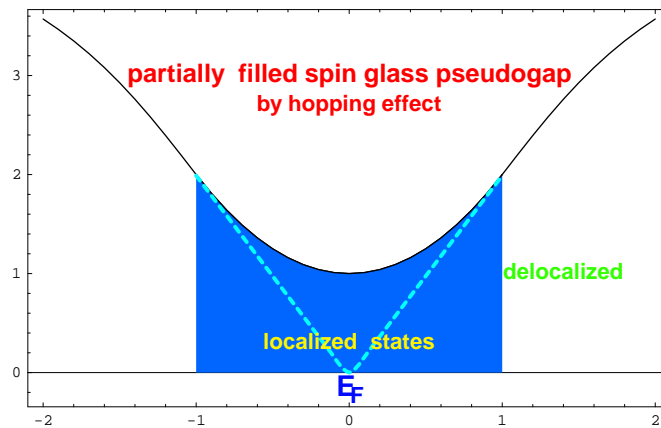


FIG. 23. Expected weak filling of the spin glass pseudogap by fermion hopping in non half-filled systems; the shown form is assumed and not yet based on calculation. Anderson-like localization, generated by the random magnetic interaction, is indicated in the small density of states regime. The dashed line sketches the possibility of critical depletion at the metal-insulator transition as in the Coulomb case.

This paper has focused so far on effects of fixed Hubbard couplings and the final section can neither give a comprehensive overview nor repeat with the same depth RSB- and Green function-calculation for U-distributions. We limit the detailed analysis of random-U models to effects concerning the freezing temperature, including modifications of tricritical behaviour. We discuss related physical problems which necessitate further studies in the future. A lot of interesting possibilities emerge in models with random distributions of different Hubbard-couplings or with randomly placed Hubbard centers. Examples include long-standing physical problems like the ones mentioned in the introduction and described in Refs. 3,16, as well as new problems which appear in artificially tailored systems, or in mathematical toy models which help to probe the spin glass state by means of different kinds of U-distributions. Apart from randomness, particularly interesting generalizations are sublattice structures modeling A-B alloys, for example with alternating signs of U, which allow staggered magnetic order in the sense of staggered deviations of the spin glass order parameter from its mean value. Such insulating states are nevertheless highly pregnant with competing or perhaps coexisting magnetic superconductivity (or superconducting magnetism) if only hopping processes are taken into account. To ead and Larkin³³ described disordered superconductors with smeared transition temperatures and randomly distributed couplings. They considered percolation of clusters, in which superconducting order can resist the destructive proximity effect of surrounding non-superconducting material. Below we consider a few different model classes which, according to what was achieved in the previous sections, shed some light on the interplay between randomness in U and the freezing temperature. Distributions of Hubbard couplings of the site-unrelated Wilson-Ising potential

$$P(U_i) = N^{-1} \exp(-a_2 U_i^2 - a_4 U_i^4)$$

facilitates the crossover from standard Gaussian distributions to a two level -distribution (random AB alloy). One may include site-site correlations by adding an additional Wilson-like term

$$\exp\left(-\frac{1}{2}(r_i U_i)^2\right);$$

where either r_i denotes the discretized gradient on the lattice or one may think of the continuum limit. We will restrict the discussion to cases of a correlation-free distribution, which will not invalidate the chosen form of the spin glass order parameter.

A. White noise distributed Hubbard couplings U_i

We study first the case of a local Gaussian disorder correlation (white noise) described by

$$\langle U_i - \langle U_i \rangle \rangle \langle U_j - \langle U_j \rangle \rangle = U^2 \delta_{ij} \quad (44)$$

The U-average of the replicated partition function considered by Eq.(4) can be written as

$$\int \prod_i dU_i \exp\left(-\frac{1}{2} \sum_i U_i^2\right) \exp\left[\frac{1}{4} \sum_i (U_i + U x_i) \left(\sum_{a;k} n_{iak}^2 - \sum_{a;k} \tilde{n}_{iak}^2\right)\right] R; \quad (45)$$

where R stands for the U-independent part in the partition function of Eq.7; n and \tilde{n} are shorthand notations for charge and spin operators expressed in terms of Grassmann fields, which are integrated over by means of $\int D$ (expression $n^2 - \tilde{n}^2$ coincides with the square bracket of Eq.5). One can see that for Gaussian distributions what one needs to do is to replace U by $U + U x_i$ and to perform the x_i -averages at each site.

The averaged freezing temperature can then be found from

$$T_f = \frac{1}{x} \int dx \exp\left(\frac{1 + U + U x}{2T_f}\right) \cosh\left(\frac{2U - U x}{2T_f}\right) \quad (46)$$

By the help of U-averaged selfconsistent equations the following problems can thus be answered immediately:

- i) change in freezing temperature,
- ii) can continuous transitions occur down to zero temperature,
- iii) how strong is the depression of spin glass order and of T_f by attractive interaction (negative U) in comparison

with the restoring repulsive interaction (positive U); distributions can be defined which probe this competition by the relative weight, the limit of infinitely broad Gaussian U -distributions being a special case, which should render the mean coupling $\langle U \rangle$ irrelevant, and

v) can random alloy models with special permitted $\langle U \rangle$ -values be expected to exhibit significant behaviour?

According to Eq.46, U cannot be absorbed in a μ -shift. The asymmetric U -dependence (attractive U suppress spin glass order while repulsive interactions support it) allows a crossing of the critical curves $T_f(\mu)$. As one can further observe in Fig.24, the critical temperature $T_f(\mu)$ averages over the competing effects of positive and negative U and varies little for broad distributions.

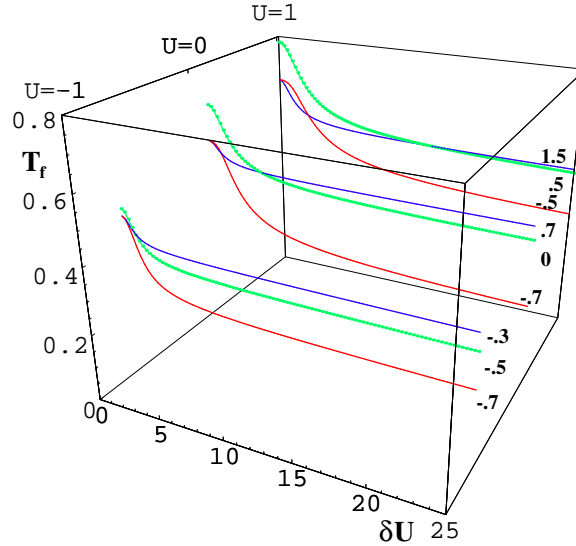


FIG.24. The variation of the freezing temperature T_f under increased variance δU of the Gaussian U -distribution is shown for three chosen values of the Hubbard coupling, $U = -1$ (attractive), $U = 0$, and $U = 1$ (repulsive). For each U , $T_f(\mu)$ is shown for three different chemical potentials (μ -value given at the right end of T_f -curve), which are symmetrically placed around the half-filling condition $\mu = U/2$ for $U = 0$.

The selfconsistency equation for T_f is simplified for $U \gg 1$ and reads

$$T_f = 1 = \frac{h}{2} + e^{(\mu - U/2)/T_f} \quad (47)$$

which is U -independent because of the infinitely broad distribution. The freezing temperature approaches $T_f(\mu) = \frac{1}{2}$ for $\mu \gg 1$ but drops discontinuously to zero near the stability limit at $\mu_{s.l.} = 0.7315$ as shown in Figure 25.

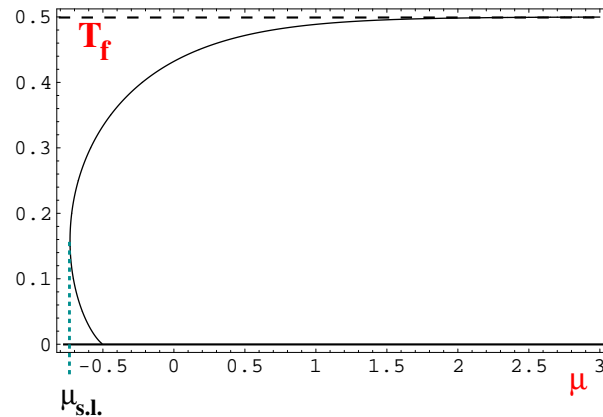


FIG.25. Solution of T_f in the limit of infinitely broad Gaussian distribution of U : one finds $T_f = \frac{1}{2}$ in the limit of large $\mu \gg 1$ while, in the small μ -regime, a stability limit shows up at $\mu_{s.l.} = 0.7315$ and implies a discontinuous drop to $T_f = 0$.

The limits $U \gg 1$ and $\mu \gg 1$ do not commute. For fixed U -variance and arbitrary U one finds that the freezing temperature decreases exponentially for $\mu \gg 1$.

For several differently chosen distributions the averaged T_f -equation results in Figure 26 showing an exponential decay in the large μ -limit of the critical temperature (for fixed U). A universal temperature $T_{f0} = T_f(\mu_0)$ is observed, where T_{f0} is independent of distributions which are symmetric with respect to U . The value μ_0 of this invariant point depends linearly on U and obeys $\mu_0(U) = 0.9939(U + 0.8626)$. One may check that the critical temperature T_f given by Eq. 24 and Figure 1 at μ_0 agrees too.

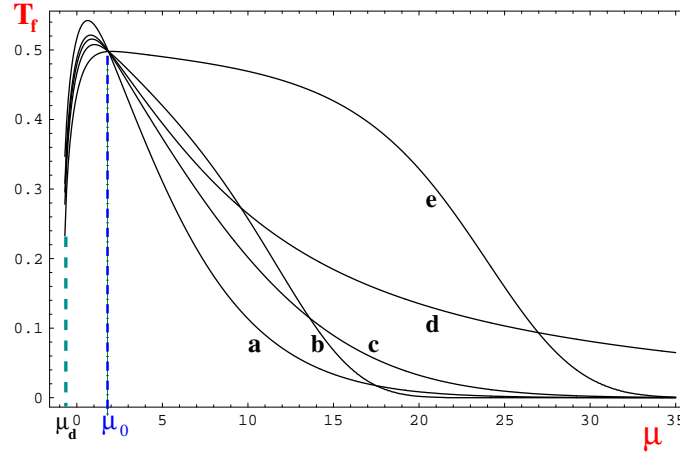


FIG. 26. Exponential decay of T_f for the normalized U -distributions a) $\exp(-x^2/2) = (x^2 + 1)^{-1}$, b) $\exp(-x^2/2) = (x^2 + 1)^{-1}$, c) $\exp(-x^2/2) = (x^2 + 1)^{-1}$, d) $\exp(-x^2/2) = (x^2 + 1)^{-1}$, and e) $\exp(-x^2/2) = (x^2 + 1)^{-1}$ with fixed $U = 1$.

For negative μ the freezing temperature vanishes discontinuously. A line of tricritical points exists. The exponential tails at large positive μ originate in the rare large U -regions. None of the given examples allows a continuous phase transition at $T = 0$, since T_f remains nonzero for all finite μ (allowing only a discontinuous drop to $T_f = 0$).

B. Alloy models with two different Hubbard couplings

Random alloys with only two different Hubbard couplings U_1, U_2 , which are assumed to be realized with probability w_1 and $w_2 = 1 - w_1$ respectively on each site obey

$$P(U_i) = w_1 \delta(U_i - U_1) + (1 - w_1) \delta(U_i - U_2) \quad (48)$$

In this model the spatial homogeneity of the spin glass order parameter Q remains unaffected. We observe that the T_f -solution for this model also passes through the universal point of Figure 26 provided $w_1 = \frac{1}{2}$. A highly interesting AB-alloy model with staggered Hubbard-interaction, defined with a U -distribution

$$P(U_i) = (U_i - U_A) \delta(U_i - U_A) + (U_i - U_B) \delta(U_i - U_B); \quad (49)$$

can break the spatial homogeneity of Q . In case that U_A on sublattice A is strongly negative, this sublattice will become nonmagnetic, while the range-free magnetic interaction maintains glassy order on sublattice B provided U_B is repulsive for example. When nearest neighbor hopping of sufficient strength is introduced, an extreme proximity effect between superconductivity and magnetism will result: local pairs can only become delocalized when single fermions tunnel through the magnetic sites. A strong U -dependence must be expected. In addition the strong interference of an eventually superconducting sublattice system with glassy magnetic order is a challenge for research on microscopic superconducting glass phases.

XI. ANTIFERROMAGNETIC-AND FERRIMAGNETIC GLASSY PHASES

The simplest model with range-free magnetic interaction, which nevertheless supports antiferromagnetic order, is the Korenblit-Shender model³⁵. The magnetic interaction is supposed to act only between A and B atoms, which one may imagine to sit on neighbouring sites, with a mean antiferromagnetic form together with random fluctuations.

In previous work¹⁸ we solved this model in one-step RSB and generalized it in several directions. Spin glass order parameters Q_A, Q_B within each sub-lattice differ in the glassy antiferromagnetic phase transition, and a third field is

necessary to describe the A-B coupling. In a field we found a level crossing of elements of Q_A and Q_B , which led us to define a new RSB-scheme. This scheme is allowed to be A-B asymmetric which, in the strongly A-B-asymmetric ferrimagnetic phase, turns out to be better than the standard solution. Details will be published elsewhere.

The Hubbard interaction can be built into the antiferromagnetic model in the same way as described before. Hubbard interactions U_A, U_B of different strength can enhance the A-B asymmetry. This is evident from the fact that sufficiently negative U , say on A-sites, render these sites nonmagnetic, while sites with positive U , say on B-sites, maintain glassy order. This case has very strong asymmetry and the new RSB-scheme of Ref. 18 must be considered as a candidate to describe such phases.

Such problems are left for future research. When hopping is also allowed for, superconductivity on the A-sublattice in competition with glassy magnetism on B-sites revive the problem of microscopic superconducting glasses as well.

XII. SUMMARY OF RESULTS AND OUTLOOK

We presented the analytical solution for the generating functional of a model with competing Hubbard- and frustrated range-free Ising spin interaction together with detailed numerical evaluations of the resulting self-consistency equations in order to describe relations between magnetism and electronic properties. The model was interpreted as the localized (but non-local) limit of a Hubbard model with additional frustrated spin interaction. The discrete time slicing method was, to our knowledge, used for the first time to solve a spin glass problem analytically (all integrations were performed before the continuum time limit was taken). Taking advantage of the rapid convergence of k -step replica symmetry breaking and using exact relations we drew conclusions on the 1 RSB solutions of important quantities such as the fermion propagator $G(E)$. The 2-4-step approximations were found to be close enough to the exact solution (by means of comparison with exact relations) and allowed us to identify and to eliminate artifacts of finite-step RSB in the extreme low temperature regime. By comparison of 0-, 1-, 2-, 3-, and 4-step results, we identified hierarchical energy regimes, $\epsilon^{(k)} < \epsilon^{(k+1)}$, where corrections beyond a certain k -step-approximation are negligibly small. For decreasing excitation energies above or below the Fermi level an increasing number of steps is required at $T = 0$ for good accuracy.

We found that all $T = 0$ phase transitions of the model (including its generalization to random distributions of the Hubbard coupling) are discontinuous with the exception of half-filling transitions. Those become continuous in the limit of infinite-step RSB (i.e. their discontinuities decay with increasing number of RSB-steps and vanish in the limit of 1 RSB).

The density of states around the spin glass pseudogap at E_F was found to obey the linear dependence $\rho(E) = c_1 E - E_F$ with $c_1 \approx 0.3$ in a wide gap regime and $c_1 \approx 0.13$ asymptotically close to the Fermi level. This was concluded from a fast convergence of $\rho(E)$ under increasing number of RSB-steps. The linear behaviour of ρ reminded us of the Efros-Shklovskii Coulomb-gap in two dimensions. These gaps have totally different origin: the Efros-Shklovskii gap originates in the bare Coulomb interaction (and naturally involves a dependence on space dimension) while the present one is caused by the spin glass order. In finite-range models the latter is expected to depend on space dimension predominantly through the destruction of glassy order at its lower critical dimensions for finite temperature and $T = 0$ -transitions respectively.

We believe that a renormalization group analysis acting in replica space (not in real or momentum space) will be helpful to describe the asymptotic behaviour linked to the hierarchical energy scales, which were discussed in our paper for the range-free model. Eventually a new type of RG must be created for this purpose. In accordance with general considerations³¹, Johnson and Khmel'nitskiĭ²⁹ showed for a disordered system with long-range (unscreened) Coulomb interaction how important and useful a RG-technique can be for the understanding of pseudogaps.

From our numerical analysis we predicted a set of other scaling laws. The linear decay of the density of states led us to claim a divergent slope of the Green function's real part at E_F and hence a divergence of a corresponding vertex, which results from charge conservation Ward identity³². These divergences are logarithmic and become visible only exponentially close to the Fermi level. This reminds of the extremely slow approach to equilibrium, which is usually discussed for spin dynamics. In the present case, in the absence of spin dynamics it is the quantum fermion dynamics, generated by the noncommuting fermion- and Hamilton operator, which experiences the hierarchical RSB-structure of spin glass order parameters. For the fermion concentration n_F (integrated density of states at $T = 0$) and for the related $T \rightarrow 0$ limit of the integrated Parisi function, $q_1 = \lim_{T \rightarrow 0} \int_0^1 dx q(x; T)$, we predicted $1 - q_1 \propto (U)^2$; $U > U_c$, near the half-filling transition. The transition generates an important crossover of the Fermi level from the center of a spin glass pseudogap into the Hubbard gap and hence into a deeper insulating state. We stressed its role for delocalization in itinerant models and described related scenarios for metal insulator transitions.

The present approach was intended to progress towards an analytical solution at $T = 0$ and the construction of a low temperature expansion. A generalization to fermionic spin glasses of a recent numerical study by Crisanti et al.¹⁹,

This figure "fig3.jpg" is available in "jpg" format from:

<http://arxiv.org/ps/cond-mat/0207734v1>

This figure "fig4.jpg" is available in "jpg" format from:

<http://arxiv.org/ps/cond-mat/0207734v1>

This figure "fig5.jpg" is available in "jpg" format from:

<http://arxiv.org/ps/cond-mat/0207734v1>

This figure "fig10-11.jpg" is available in "jpg" format from:

<http://arxiv.org/ps/cond-mat/0207734v1>

This figure "fig18.gif" is available in "gif" format from:

<http://arxiv.org/ps/cond-mat/0207734v1>

This figure "fig19.gif" is available in "gif" format from:

<http://arxiv.org/ps/cond-mat/0207734v1>

This figure "fig21.gif" is available in "gif" format from:

<http://arxiv.org/ps/cond-mat/0207734v1>